University of Zurich[UZH]

Zurich Open Repository and Archive
University of Zurich
University Library
Strickhofstrasse 39
CH-8057 Zurich
www.zora.uzh.ch

Year: 2020

Light-induced radiosynthesis of 89ZrDFO-azepin-onartuzumab for imaging the hepatocyte growth factor receptor

Klingler, Simon ; Fay, Rachael ; Holland, Jason P

Abstract: Methods that provide rapid access to radiolabeled antibodies are vital in the development of diagnostic and radiotherapeutic agents for positron emission tomography (PET) or radioimmunotherapy. The human hepatocyte growth factor receptor (c-MET) signaling pathway is dysregulated in a number of malignancies including gastric cancer, and is an important biomarker in drug discovery. Here, we used a photoradiochemical approach to produce 89Zr-radiolabeled onartuzumab (a monovalent, anti-human c-MET antibody), starting directly from the fully formulated drug (MetMAb). Methods: Simultaneous 89Zr-radiolabeling and protein conjugation was performed in one-pot reactions containing 89Zr-oxalate, the photoactive chelate DFO-aryl azide (DFO-ArN3) and MetMAb to give 89ZrDFO-azepin-onartuzumab. As a control, 89ZrDFO-Bn-NCS-onartuzumab was prepared via a conventional two-step process using pre-purified onartuzumab and DFO-Bn-NCS. Radiotracers were purified by using size-exclusion methods and evaluated by radiochromatography. Radiochemical stability was studied in human serum and immunoreactivity was determined by cellular binding assays using MKN-45 gastric carcinoma cells. PET imaging at multiple time points (0–72 h) was performed in female athymic nude mice bearing subcutaneous MKN-45 xenografts. Biodistribution experiments were performed after the final image. Tumor specificity of 89ZrDFO-azepin-onartuzumab was assessed by competitive inhibition (blocking) studies. Results: Initial photoradiosynthesis experiments produced 89ZrDFO-azepin-onartuzumab in <15 min. with an isolated decay-corrected radiochemical yield (RCY) of 24.8%, a radiochemical purity (RCP) 90% and a molar activity (Am) of 1.5 MBq nmol-1. Reaction optimization improved the radiochemical conversion (RCC) of 89ZrDFO-azepin-onartuzumab to 56.9±4.1% (n = 3), with isolated RCYs of 41.2±10.6% (n = 3), and RCPs >90%. Conventional methods produced 89ZrDFO-Bn-NCS-onartuzumab with isolated RCY >97%, RCP >97% and Am 14.0 MBq nmol-1. Both radiotracers were immunoreactive and stable in human serum. PET imaging and biodistribution studies showed high tumor uptake for both radiotracers. By 72 h, tumor and liver uptake reached 15.37±5.21 %ID g-1, 6.56±4.03 %ID g-1, respectively for 89ZrDFO-azepin-onartuzumab (n = 4), and 21.38±11.57 %ID g-1 and 18.84±6.03 %ID g-1 for 89ZrDFO-Bn-NCS-onartuzumab (n = 4). Blocking experiments gave a statistically significant reduction in tumor uptake (6.34±0.47 %ID g-1) of 89ZrDFO-azepin-onartuzumab (n = 4). Conclusion: Experiments demonstrate that photoradiosynthesis is a viable alternative approach for producing 89Zr-radiolabeled antibodies direct in protein formulation buffer which reduces protein aggregation and liver uptake.

DOI: https://doi.org/10.2967/jnumed.119.237180

Posted at the Zurich Open Repository and Archive, University of Zurich
ZORA URL: https://doi.org/10.5167/uzh-186990
Journal Article
Accepted Version

Originally published at:
Klingler, Simon; Fay, Rachael; Holland, Jason P (2020). Light-induced radiosynthesis of 89ZrDFO-azepin-onartuzumab for imaging the hepatocyte growth factor receptor. Journal of Nuclear Medicine, 61(7):1072-1078.
DOI: https://doi.org/10.2967/jnumed.119.237180

Light-induced radiosynthesis of ^{89}ZrDFO-azepin-onartuzumab for imaging the hepatocyte growth factor receptor

Simon Klingler, Rachael Fay and Jason P. Holland*

University of Zurich, Department of Chemistry, Winterthurerstrasse 190, CH-8057, Zurich, Switzerland

*** Corresponding Author:**

Prof. Dr Jason P. Holland

Tel: +41.44.63.53.990

E-mail: jason.holland@chem.uzh.ch

Website: www.hollandlab.org

First author:

Simon Klingler

E-mail: simon.klingler@chem.uzh.ch

Running Title: *Photoradiosynthesis of ^{89}Zr-antibodies*

Words (Main text): 4997

ABSTRACT

Methods that provide rapid access to radiolabeled antibodies are vital in the development of diagnostic and radiotherapeutic agents for positron emission tomography (PET) or radioimmunotherapy. The human hepatocyte growth factor receptor (c-MET) signaling pathway is dysregulated in a number of malignancies including gastric cancer, and is an important biomarker in drug discovery. Here, we used a photoradiochemical approach to produce ^{89}Zr-radiolabeled onartuzumab (a monovalent, anti-human c-MET antibody), starting directly from the fully formulated drug (MetMAb).

Methods: Simultaneous ^{89}Zr-radiolabeling and protein conjugation was performed in one-pot reactions containing ^{89}Zr-oxalate, the photoactive chelate DFO-aryl azide (DFO-ArN_3) and MetMAb to give ^{89}ZrDFO-azepin-onartuzumab. As a control, ^{89}ZrDFO-Bn-NCS-onartuzumab was prepared *via* a conventional two-step process using pre-purified onartuzumab and DFO-Bn-NCS. Radiotracers were purified by using size-exclusion methods and evaluated by radiochromatography. Radiochemical stability was studied in human serum and immunoreactivity was determined by cellular binding assays using MKN-45 gastric carcinoma cells. PET imaging at multiple time points (0–72 h) was performed in female athymic nude mice bearing subcutaneous MKN-45 xenografts. Biodistribution experiments were performed after the final image. Tumor specificity of ^{89}ZrDFO-azepin-onartuzumab was assessed by competitive inhibition (blocking) studies.

Results: Initial photoradiosynthesis experiments produced ^{89}ZrDFO-azepin-onartuzumab in <15 min. with an isolated decay-corrected radiochemical yield (RCY) of 24.8%, a radiochemical purity (RCP) ~90% and a molar activity (A_m) of ~1.5 MBq nmol^{-1}. Reaction optimization improved the radiochemical conversion (RCC) of ^{89}ZrDFO-azepin-onartuzumab to 56.9±4.1% (n = 3), with

isolated RCYs of 41.2±10.6% (n = 3), and RCPs >90%. Conventional methods produced ^{89}ZrDFO-Bn-NCS-onartuzumab with isolated RCY >97%, RCP >97% and A_m ~14.0 MBq nmol^{-1}. Both radiotracers were immunoreactive and stable in human serum. PET imaging and biodistribution studies showed high tumor uptake for both radiotracers. By 72 h, tumor and liver uptake reached 15.37±5.21 %ID g^{-1}, 6.56±4.03 %ID g^{-1}, respectively for ^{89}ZrDFO-azepin-onartuzumab (n=4), and 21.38±11.57 %ID g^{-1} and 18.84±6.03 %ID g^{-1} for ^{89}ZrDFO-Bn-NCS-onartuzumab (n=4). Blocking experiments gave a statistically significant reduction in tumor uptake (6.34±0.47 %ID g^{-1}) of ^{89}ZrDFO-azepin-onartuzumab (n=4).

Conclusions: Experiments demonstrate that photoradiosynthesis is a viable alternative approach for producing ^{89}Zr-radiolabeled antibodies direct in protein formulation buffer which reduces protein aggregation and liver uptake.

Keywords: Photoradiosynthesis, immuno-PET, antibodies, hepatocyte growth factor receptor (c-MET), zirconium-89, MetMAb, onartuzumab

INTRODUCTION

Monoclonal antibodies (mAbs) radiolabeled with ^{89}Zr are important tools for non-invasive immuno-positron emission tomography (immuno-PET) of biomarker fluctuations during cancer diagnosis, progression and treatment. Existing methods to produce clinical-grade ^{89}Zr-radiolabeled mAbs rely on multiple step processes. First, the protein is purified to remove formulation components that can interfere with the subsequent chemistry. Second, the mAb is functionalized with the chelate desferrioxamine B (DFO) and then re-purified to remove unreacted coupling reagents. Functionalization typically occurs by reacting the ε-NH_2 of lysine residues forming amide bond with the activated ester of DFO-succinate,(*1*,*2*) or thioureas with DFO-Bn-NCS.(*3*) Importantly, the functionalized mAb is then characterized and stored (typically in saline, PBS or HEPES buffer) prior to ^{89}Zr-radiolabeling.

Current ^{89}Zr-radiochemistry processes are highly successful and many ^{89}Zr-radiolabeled mAbs have been evaluated in the clinic.(*4*) However, the radiosynthesis and characterization of ^{89}Zr-radiolabeled mAbs remains non-trivial, and production is restricted to specialist facilities. Automated synthesis and purification methods are likely to improve access to ^{89}Zr-radiolabel mAbs(*5*) but other physical and regulatory issues associated with the isolation, characterization and long-term storage of the functionalized intermediate mAb are more challenging to address with existing chemistry. Antibody functionalization may alter the biophysical properties of the protein, and storage leads to questions over the long-term stability and viability of the radiolabeling precursor. These issues mean than some regulatory authorities require absorption, distribution, metabolism, excretion and toxicological (ADME-tox) profiling of the functionalized intermediate. Providing ADME-tox data entails both technical and financial challenges – producing enough

functionalized protein is non-trivial and requires a considerable, and often prohibitive, capital investment. Methods that avoid isolation of an intermediate are potentially advantageous.

Cellular signaling by the human hepatocyte growth factor receptor (c-MET) pathway is dysregulated in various human cancers including gastric, breast, lung, ovarian and pancreatic cancer.(*6*) Dysregulation can occur in the form of overexpression and amplification of the c-MET gene which induces signaling cascades that influence tumor proliferation *via* the P13K/AKT and Ras/MAPK pathways.(*7*) Several MET inhibitors and anti-MET antibodies are under evaluation and imaging of c-MET expression has the potential to support the clinical trials of MET-targeted therapies.(*8–11*)

Onartuzumab, (MetMAb, Genentech Inc. [Roche Group], South San Francisco, CA) is a humanized, one-armed monovalent anti-human c-MET antibody designed to bind the extracellular domain of c-MET and block activation by the hepatocyte growth factor (HGF; also known as scatter factor).(*12*) The monovalent design of onartuzumab was employed to avoid dimerization and activation of the c-MET receptor which leads to pro-angiogenic signal transduction.(*13*) MetMAb has been investigated in phase III trials(*14*) as a treatment for non-small-cell lung cancer (NSCLC) and onartuzumab has been used for immuno-PET with ^{89}Zr or ^{76}Br radionuclides, and for radioimmunotherapy with ^{177}Lu.(*8–11*)

Our group has recently developed a one-pot photoradiosynthesis approach for the simultaneous conjugation and ^{89}Zr-radiolabeling of mAbs.(*15–19*) Here, we evaluated the photoradiosynthesis of ^{89}Zr-radiolabeled onartuzumab starting from fully formulated MetMAb without pre-purification of the protein or isolation of an intermediate (Figure 1).

MATERIALS AND METHODS

Full details are presented in the supporting information.

Antibody Samples

Onartuzumab (MW=99.16 kDa; 66 Lys; molar absorption coefficient, ε_{280}=161,465 M^{-1} cm^{-1}) was supplied by Genentech as the formulated drug (MetMAb). Stock solutions of MetMAb contained a protein concentration of 60 mg mL^{-1} formulated in 10 mmol L^{-1} histidine succinate, 106 mmol L^{-1} trehalose dihydrate, and 0.02% polysorbate 20 at pH5.7. Protein samples were aliquoted and stored at -70ºC.(*20*)

Synthesis, Photochemistry and Radiochemistry

$[^{89}Zr][Zr(C_2O_4)_4]^{4-}$(aq.) was obtained as a solution in ~1.0 M oxalic acid from PerkinElmer (Boston, MA, manufactured in The Netherlands) and was used without further purification. Conjugation and radiolabeling of DFO-Bn-NCS-onartuzumab was performed in accordance with previously reported methods.(*3*) The photoactive chelate DFO-ArN_3 was synthesised and characterized previously and photoradiochemical conjugation reactions were performed in accordance with methods reported by Patra *et al*.(*17*) Note the compound undergoes slow degradation over ~4 months at -20ºC. Fresh samples should be isolated prior to use.

Stability Studies

The stability of ^{89}Zr-DFO-azepin-onartuzumab and ^{89}Zr-DFO-Bn-NCS-onartuzumab with respect to change in radiochemical purity, loss of radioactivity from the mAb and/or change in immunoreactivity was investigated *in vitro* by incubation in solutions of human serum for 48h at

37ºC. The radiochemical purity was determined by radiochromatography using a size-exclusion column coupled to a high-performance liquid chromatography system (HPLC).

Cell Binding Assays

For cell binding assays, the human gastric cancer cell line MKN-45 (c-MET overexpressing, Leibniz Institute DSMZ-German collection of Microorganisms and Cell cultures [ACC-409]) was used. Immunoreactivity was determined using a procedure adapted from Lindmo *et al*.(*21*)

Animals and Xenograft Models

Animal experiments were conducted in accordance with an experimentation licence approved by the Zurich Canton Veterinary Office, Switzerland. Female athymic nude mice (Crl:NU(NCr)-*Foxn1*^{nu}, 20–25 g, 4–8 weeks old) were obtained from Charles River Laboratories Inc. (Freiburg im Breisgau, Germany). Tumours were induced on the right shoulder or flank by sub-cutaneous (s.c.) injection of approx. 2.5×10^6 cells suspended in 200 µL of a 1:1 v/v mixture of PBS and reconstituted basement membrane (Corning® Matrigel® Basement Membrane Matrix, obtained from VWR International).(*22*)

Small-Animal PET Imaging

PET imaging experiments were conducted on a Genesis G4 PET/X-ray scanner (Sofie Biosciences, Culver City, CA). Radiotracers were administered 200 µL sterile PBS by intravenous (i.v.) tail-vein injection (t=0 h). Approximately 5 minutes prior to recording PET images, mice were anesthetized by inhalation of 2-3% isoflurane (Baxter Healthcare, Deerfield, IL)/oxygen gas

mixture (~5 L/min) and placed on the scanner bed. PET images were recorded at various time-points between 0–72 h post-injection (see supporting information for full details).

Biodistribution Studies

Tumor-bearing mice were randomized before the study. Animals (n=4, per group) were euthanized by exsanguination under anaesthesia. Tissue samples were removed, rinsed in water, dried in air for ~2 min., weighed and counted on a gamma-counter for accumulation of ^{89}Zr-radioactivity. Full details are presented in the supporting information.

Statistical Analysis

Data were analyzed by using the unpaired, two-tailed Student's t-test. Differences at the 95% confidence level (P<0.05) were considered to be statistically significant.

RESULTS

Radiochemistry

The synthesis, characterization, and reactivity of the photoactive chelate DFO-ArN_3 (**1**) was reported elsewhere.(*17*) Briefly, a neutralized stock solution of $[^{89}Zr(C_2O_4)_4]^{4-}$ (^{89}Zr-oxalate) was added to an open glass vial containing a mixture of compound **1** and formulated onartuzumab with an initial chelate-to-mAb ratio of 6.15-to-1, and a final pH ~8–9. The reaction was stirred gently at room temperature and irradiated directly for 10 min. by using a light emitting diode source (LED, λ_{max}=364.5 nm, FWHM=9.1 nm, power=263 mW, Supplemental Figure 1). Prior tests determined that this experimental geometry was sufficient to affect complete photochemical reaction of DFO-ArN_3.(*17*) After quenching the reaction with excess DTPA to ensure that any free

$^{89}Zr^{4+}$ ions that may non-specifically bind to proteins were solubilized, crude aliquots were analyzed by radioactive instant thin-layer chromatography (radio-iTLC; Supplemental Figure 2), manual size-exclusion chromatography (SEC) using PD-10 gel filtration columns (Figure 2A), and high-performance liquid chromatography coupled to a size exclusion gel column (SEC-HPLC; Figure 2B). Chromatographic methods on the crude reaction samples confirmed that ^{89}Zr-activity was bound to the protein as evidenced by a peak in the PD-10 chromatograms in the 0.0–1.6 mL fraction (radiochemical conversion, RCC ~25.0%, Figure 2A red trace) and by a radioactive peak in the SEC-HPLC that coincided with the retention time of onartuzumab at ~14.1 min. (RCC ~35.0%, Figure 2B red trace). A fraction of the reaction mixture was purified manually by using preparative PD-10 SEC and aliquots of the purified sample were reanalyzed using the same chromatographic methods (Figure 2, and Supplemental Figure 2, green traces). After purification, the photoradiochemically synthesized product, ^{89}ZrDFO-azepin-onartuzumab was isolated with a decay-corrected radiochemical yield (RCY) of 24.8%, and a radiochemical purity of ~90% as measured by both analytical PD-10 SEC, and by SEC-HPLC. The final molar activity was ~1.5MBq nmol^{-1} of protein at an activity concentration of 3.87MBq mL^{-1}.

As a control for use in the biological assays that followed, we also prepared ^{89}ZrDFO-Bn-NCS-onartuzumab *via* a traditional multiple step procedure that involved pre-purification of onartuzumab from the formulation buffer, functionalization with the commercially available DFO-Bn-NCS reagent, and subsequent ^{89}Zr-radiolabeling of the purified intermediate using established methods.(*1*,*2*) For comparison, crude and purified aliquots of ^{89}ZrDFO-Bn-NCS-onartuzumab were tested using the same chromatographic methods as described above (Figure 2 and Supplemental Figure 2, crude samples = black traces, purified samples = blue traces). ^{89}ZrDFO-Bn-NCS-onartuzumab was obtained with an isolated decay-corrected RCY of >97%, a RCP >97%

(measured by both analytical PD-10 SEC and by SEC-HPLC), a molar activity of ~14.0MBq nmol^{-1} of protein, and an activity concentration of ~19.0MBq mL^{-1}. The radiochemical purity of ^{89}ZrDFO-Bn-NCS-onartuzumab was higher than that of ^{89}ZrDFO-azepin-onartuzumab produced by photoradiosynthesis primarily because the efficiency of the PD-10 columns decreased when separating a larger fraction of radioactive 'small-molecules' from the labeled protein, and also because the pore size and loading capacity of standard 2.5 mL PD-10 columns provides insufficient resolution. This issue can be readily resolved by using larger gel filtration columns, alternative gels with finer particle sizes, or by switching to spin-column SEC methods.

Purified samples of ^{89}ZrDFO-Bn-NCS-onartuzumab produced *via* the conventional multiple step route contained ~24% of aggregated protein which increased from ~15% in the crude mixtures (Figure 2B, asterisk). In contrast, photoradiosynthesis of ^{89}ZrDFO-azepin-onartuzumab using formulated MetMAb gave an aggregated protein fraction of <4% in the final product.

Stability Studies

Isolated samples of ^{89}ZrDFO-azepin-onartuzumab and ^{89}ZrDFO-Bn-NCS-onartuzumab were incubated in human serum at 37ºC for up to 48h. Radiochemical chemical stability with respect to loss of ^{89}Zr activity from the protein fraction was analyzed by SEC-HPLC (Supplemental Figure 3). Both radiotracers were found to be stable under these conditions with essentially no loss of ^{89}Zr-activity from the mAb.

Cellular Binding and Immunoreactivity

The binding and specificity of ^{89}ZrDFO-azepin-onartuzumab and ^{89}ZrDFO-Bn-NCS-onartuzumab to the target protein was evaluated *in vitro* by using cellular association assays with

c-MET positive and overexpressing MKN-45 gastric adenocarcinoma cells (Supplemental Figure 4). Blocking studies with excess MetMAb confirmed the binding specificity, and standard Lindmo transformations gave immunoreactive fractions of 38% for ^{89}ZrDFO-azepin-onartuzumab and 54% for ^{89}ZrDFO-Bn-NCS-onartuzumab.(*21*) The relatively low immunoreactive fractions for both radiotracers was consistent with our previous characterization data using ^{68}GaHBED-CC-azepin-onartuzumab(*18*) and is likely due to the well-documented limitations of the Lindmo assay.(*23–25*)

Radiochemical Optimization

A series of photoradiolabeling experiments were performed to optimize the reaction parameters and obtain higher isolated RCYs of ^{89}ZrDFO-azepin-onartuzumab. The effect of changing the initial chelate-to-mAb ratio and the initial protein concentration are shown in Figure 3A and 3B, respectively (see also Supplemental Table 1). After optimization, the radiochemical conversion to give ^{89}ZrDFO-azepin-onartuzumab was improved to an average of 58.1±3.4% (*n*=10; measured by SEC-HPLC), with an isolated decay-corrected RCY of 36.6±10.3% (*n*=9), and an average RCP of 91.2±1.1% (*n*=9; measured by SEC-HPLC). The effect of not stirring the reaction was also measured and a RCY of 56.5% was obtained indicating that stirring the solutions had no influence in our experimental geometry. Experiments showed that by using initial chelate-to-mAb ratios ranging from 4.62 to 0.77 had no effect on the RCY. In contrast, the reaction was very sensitive to changes in protein concentration. When the initial protein concentrations were reduced to ≤12μM, the measured RCYs decreased dramatically to <30%, and for protein concentrations ≤1μM, RCYs ranged between 5.6% to 13.7% (*n*=4; Supplemental Table 1).

PET Imaging

Temporal immuno-PET imaging of ^{89}ZrDFO-Bn-NCS-onartuzumab and photoradiolabeled ^{89}ZrDFO-azepin-onartuzumab was performed female athymic nude mice bearing subcutaneous MKN-45 xenografts on the right flank/shoulder (*n*=4 mice/group). A third group of animals (*n*=4 mice) received a low molar activity formulation of the same batch of photoradiolabeled ^{89}ZrDFO-azepin-onartuzumab diluted with non-radioactive MetMAb as a blocking group control to measure the specificity of tumor uptake *in vivo*. PET images recorded at 6h and 72h post-radiotracer administration are shown in Figure 4 and further tomographic and maximum intensity projection (MIP) images are shown Supplemental Figures 5 and 6, respectively. Image quantification based on volume-of-interest (VOI) analysis with data presented in units of percentage injected dose per cubic centimeter (%ID cm^{-3}) are shown in Figure 5 and Supplemental Figure 7. PET imaging revealed that photoradiolabeled ^{89}ZrDFO-azepin-onartuzumab is a viable radiotracer for quantifying c-MET expression *in vivo*. ^{89}ZrDFO-azepin-onartuzumab displayed a prolonged circulation time and specific tumor uptake that increased from 8.8±0.5%ID cm^{-3} after 6 h to 13.7±2.9%ID cm^{-3} at 72 h post-administration. Tumor uptake of ^{89}ZrDFO-azepin-onartuzumab in the blocking group showed a statistically significant difference with only 4.3±2.2%ID cm^{-3} after 6 h (Student's *t*-test *P*-value=0.023) and peak at only 6.6±2.4%ID cm^{-3} at 72h (*P*-value=0.001). In comparison, tumor-associated uptake of ^{89}ZrDFO-Bn-NCS-onartuzumab showed a higher overall uptake and increased from 14.3±1.7%ID cm^{-3} after 6h (*P*-value *versus* the normal photoradiolabeled group = 0.005) to 19.7±4.8%ID cm^{-3} by 72h (*P*-value=0.088). Notably, by 72h no statistically significant difference was observed between the tumor uptake of the two radiotracers.

Quantitative analysis of the PET images also revealed a statistically significant lower accumulation of ^{89}Zr activity in the liver for ^{89}ZrDFO-azepin-onartuzumab (7.5±2.8%ID cm^{-3}) *versus* ^{89}ZrDFO-Bn-NCS-onartuzumab at 72h (17.8±4.0%ID cm^{-3}; *P*-value=0.007). For the ^{89}ZrDFO-azepin-onartuzumab blocking group, the additional administered mass of protein led to an increased accumulation and retention of ^{89}Zr activity in the kidneys (18.9±7.5%ID cm^{-3} versus 8.5±0.7%ID cm^{-3} for the normal group at 72h; *P*-value=0.05). A similar dose-dependent change in kidneys uptake was observed for ^{68}GaHBED-CC-azepin-onartuzumab confirming that this phenomenon is unrelated to the radionuclide or chelate.(*18*)

Effective Half-life Measurements

Whole-body activity was measured in each mouse by using a dose calibrator to determine the effective ($t_{1/2}$(eff)/h) and biological ($t_{1/2}$(biol)/h) half-lives of the two radiotracers (Supplemental Figure 8). ^{89}ZrDFO-azepin-onartuzumab had a $t_{1/2}$(eff)=21.8±4.3h and a calculated $t_{1/2}$(biol)=30.2±10.8h compared with $t_{1/2}$(eff)=31.9±5.6h and $t_{1/2}$(biol)=53.8±5.6h for ^{89}ZrDFO-Bn-NCS-onartuzumab. No difference was observed in the measured values of $t_{1/2}$(eff) for the normal and blocking groups of ^{89}ZrDFO-azepin-onartuzumab which confirmed that even though kidney uptake increased in animals that received a blocking dose of MetMAb, whole-body radiotracer excretion did not change.

Biodistribution Studies

After the final imaging time point at 72h, animals were euthanized by terminal exsanguination under anesthesia and 15 tissues, including the tumors, were collected for accurate quantification of the accumulated ^{89}Zr activity (Figure 6, Supplemental Table 2 and Supplemental Figures 9 and

10). Biodistribution data are consistent with the distribution patterns observed from the quantitative PET. Measured accumulation of activity in the tumor and liver was 15.4±5.2%ID g^{-1} and 6.6±4.0%ID g^{-1}, for ^{89}ZrDFO-azepin-onartuzumab respectively, whereas for ^{89}ZrDFO-Bn-NCS-onartuzumab uptake values were 21.4±11.6%ID g^{-1} and 18.8±6.0%ID g^{-1}, respectively. With the exception of the activity accumulation in the liver and spleen (*P*-value=0.018 and 0.022), no statistically significant differences were observed between the ^{89}ZrDFO-azepin-onartuzumab and ^{89}ZrDFO-Bn-NCS-onartuzumab groups. Comparison of the tumor-associated activity for the normal and blocking groups (6.3±1.0%ID g^{-1}) that received ^{89}ZrDFO-azepin-onartuzumab confirmed that tumor uptake for the photoradiolabeled product was specific (*P*-value=0.03). No statistically significant differences were observed in the measured tumor-to-tissue contrast ratios between the conventional and photoradiolabeled products (Supplemental Figure 10). Overall, the cellular assays, PET imaging, and biodistribution data confirm that both ^{89}ZrDFO-azepin-onartuzumab and ^{89}ZrDFO-Bn-NCS-onartuzumab are viable radiotracers for measuring c-MET protein expression in gastric adenocarcinomas.

DISCUSSION

Extensive spectroscopic and computational studies have established the mechanism of photochemical activation of the ArN_3 group and comprehensive details are given in our previous reports.(*15–17*,*19*) Briefly, light-induced activation of the $[^{89}ZrDFO\text{-}ArN_3]^+$ produces the highly reactive open-shell singlet nitrene (life time, τ ~1 ns). This nitrene species is too short-lived to undergo efficient bimolecular chemistry with the protein (or indeed the solvent). Instead, the singlet nitrene undergoes rapid intramolecular rearrangement to give first a bicyclic benzazirene which then ring-opens to give a 7-membered ketenimine heterocycle which acts as the key

electrophilic intermediate.(*26–29*) Remarkably, this ketenimine intermediate reacts preferentially with primary (and secondary) amines over oxygen-based nucleophiles with a low kinetic barrier (~50 kJ mol^{-1}) that is thermally accessible under ambient conditions. This phenomenon favors bimolecular reactions with the comparatively low levels of protein over background quenching reactions.

Advantages of using our photoradiosynthesis approach to produce ^{89}Zr-radiolabeled mAbs include: *i*) Rapid reaction kinetics where both the radiolabeling and protein conjugation steps occur at the same time and are complete in <10 min.(*30*) *ii*) Chemoselective functionalization of lysine side-chains by nucleophilic attack on the electrophilic ketenimine intermediate.(*26*,*28*) *iii*) Tolerance of the photochemical process to water, oxygen, salts and clinical-grade mAb formulation buffers (including histidine) that are essential to maintain protein stability. Our experimental data recorded *in vitro* and *in vivo* support this statement where ^{89}ZrDFO-azepin-onartuzumab exhibits a lower degree of protein aggregation and decreased accumulation of ^{89}Zr activity in the liver compared to ^{89}ZrDFO-Bn-NCS-onartuzumab. *iv*) Photoactivation occurs at wavelengths where antibodies do not absorb. Hence, the photoreaction does not damage the structure and function of the biological vector.(*18*) *v*) Unlike conventional methods, photoradiosynthesis is amenable to full automation which may streamline the efforts required to produce ^{89}Zr-mAbs. Finally, *vi*) the one-pot photoradiosynthesis procedure produces formulated ^{89}Zr-mAbs without the need to isolate, characterize and store the functionalized intermediates. This novel concept has the potential to change the way in which ^{89}Zr-mAbs are produced in the clinic because it eliminates issues over the long-term stability of the functionalized intermediates and circumvents the technical and financial issues of performing ADME-tox studies on the intermediate.

In spite of the many attractive features, photoradiosynthesis of ^{89}Zr-mAbs has several limitations that require further research. Prior experiments using different photoactive chelates, radionuclides and proteins have revealed strong variations in the radiochemical conversions and isolated RCYs. Photoradiosynthesis using [^{89}ZrDFO-ArN_3]$^+$ has (so far) afforded the highest RCCs with values in this study peaking at 58.1±3.4% and in previous work ^{89}ZrDFO-azepin-trastuzumab was obtained in RCCs of 67% to 88%.(*17*) Studies using $^{68}Ga^{3+}$ and $^{111}In^{3+}$ radionuclides combined with either *aza*-macrocyclic or acyclic chelates afforded lower photo-induced RCCs in the range 4% to ~25%.(*15*,*16*,*18*,*19*) The light-induced chemistry is highly dependent on the experimental geometry. Although kinetic studies have shown that the photo-initiation step is highly efficient, and linearly dependent on photon flux,(*15*,*17*) the photon beam shape, focal point, reaction volume, and potential scattering or absorption of the incident light by the reaction vessel or chemical components in the mixture can have a dramatic impact on the observed RCCs. Experimental RCCs also show a steep dependency on the initial protein concentration.

Another issue is the poor solubility of DFO-ArN_3 in aqueous conditions – it dissolves at high pH>10 but precipitates readily on adjusting the pH to the optimum window of between 7.5–9.0 required for the photochemical reaction.(*17*) Higher pH values cannot be used because many antibodies do not tolerate highly basic conditions, and our experiments have found that at pH~9.0, the measured RCCs decrease due to hydrolysis of the ketenimine intermediate by hydroxide anions. The solubility issues associated with DFO-ArN_3 can potentially be addressed by using the strategy of Codd and co-workers(*31*) who incorporated ether groups in the chelate backbone, or by the addition of polyethylene glycol (PEG) chains between the chelate and the photoactive ArN_3 group.(*15*,*16*) At present, variations in the RCCs are also the main reason why it is more difficult

to purify the ^{89}Zr-mAb from the photochemical reaction mixture than from conventional syntheses that often show quantitative radiolabeling. These purification issues are primarily technical in nature and can be solved by using alternative purification methods such as spin column centrifugation. Nevertheless, improving the reaction efficiency remains our primary goal. Much work remains before photoradiosynthetic methods can be standardized. However, the results presented here demonstrate that photoradiosynthesis – starting from formulated antibody stock solutions – yields viable radiotracers which sets an important and encouraging precedent for future use of this technology in Nuclear Medicine.

CONCLUSION

^{89}Zr-radiolabeled onartuzumab was produced via two separate synthesis routes involving traditional thermally-mediated conjugation using isothiocyanate (NCS) chemistry and an alternative light-induced photochemical conjugation process using aryl azide (ArN_3) chemistry. These approaches yielded ^{89}ZrDFO-Bn-NCS-onartuzumab and ^{89}ZrDFO-azepin-onartuzumab which were both shown to be viable radiotracers targeting the c-MET receptor in gastric adenocarcinoma. Switching the synthesis to a simultaneous, one-pot photochemical conjugation and ^{89}Zr-radiolabeling route has the advantage that the photochemistry is compatible with standard components of antibody formulation buffers. The photoradiosynthesis was also completed in <15 min. and gave a final product that displayed a decreased tendency toward protein aggregation, and consequently lower uptake in the liver and spleen. Radiochemical conversions were systematically improved by investigating different reaction parameters including the initial chelate-to-antibody ratio and the protein concentration. Further studies are required to improve the isolated radiochemical yield, radiochemical purity, and molar activity of the final products but these data

encourage the development of photoradiosynthesis as an alternative labeling strategy for the production of clinical-grade ^{89}Zr-radiolabeled proteins.

ACKNOWLEDGMENTS

JPH thanks the Swiss National Science Foundation (SNSF Professorship PP00P2_163683 and PP00P2_190093), the Swiss Cancer League (Krebsliga Schweiz; KLS-4257-08-2017), and the University of Zurich (UZH) for financial support. This project has received funding from the European Union's Horizon 2020 research and innovation programme / from the European Research Council under the Grant Agreement No 676904, ERC-StG-2015, NanoSCAN. We thank all members of the Radiochemistry and Imaging Science group at UZH for helpful discussions, and Melanie Gut for technical assistance with the imaging and biodistribution experiments.

Conflicts of Interest

No potential conflicts of interest relevant to this article exist.

Key points

Question: Can photochemical methods be used to produce viable radiopharmaceuticals for immuno-PET?

Pertinent findings: Experiments demonstrate that a one-pot, simultaneous light-induced chemical conjugation and radiolabeling process can produce ^{89}ZrDFO-azepin-onartuzumab for imaging c-MET receptors, starting directly from a fully formulated solution of MetMAb.

Implications for patient care: New methods to access radiolabeled antibodies has the potential to increase the availability of radiotracers for immuno-PET and to improve the stability of the final radiolabeled constructs.

REFERENCES

1. Verel I, Visser GWM, Boellaard R, Stigter-van Walsum M, Snow GB, van Dongen GAMS. 89Zr immuno-PET: comprehensive procedures for the production of 89Zr-labeled monoclonal antibodies. *J Nucl Med*. 2003;44:1271-81.

2. Holland JP, Divilov V, Bander NH, Smith-Jones PM, Larson SM, Lewis JS. 89Zr-DFO-J591 for ImmunoPET of Prostate-Specific Membrane Antigen Expression In Vivo. *J Nucl Med*. 2010;51:1293-1300.

3. Vosjan MJWD, Perk LR, Visser GWM, et al. Conjugation and radiolabeling of monoclonal antibodies with zirconium-89 for PET imaging using the bifunctional chelate p-isothiocyanatobenzyl-desferrioxamine. *Nat Protoc*. 2010;5:739-743.

4. Bensch F, Smeenk MM, van Es SC, et al. Comparative biodistribution analysis across four different 89Zr-monoclonal antibody tracers-The first step towards an imaging warehouse. *Theranostics*. 2018;8:4295-4304.

5. Poot AJ, Adamzek KWA, Windhorst AD, et al. Fully automated zirconium-89 labeling and purification of antibodies. *J Nucl Med*. 2019;60:691-695.

6. Peruzzi B, Bottaro DP. Targeting the c-Met signaling pathway in cancer. *Clin Cancer Res*. 2006;12:3657-3660.

7. Zhang Y, Xia M, Jin K, et al. Function of the c-Met receptor tyrosine kinase in carcinogenesis and associated therapeutic opportunities. *Mol Cancer*. 2018;17:1-14.

8. Han Z, Xiao Y, Wang K, et al. Development of a SPECT Tracer to Image c-Met Expression in a Xenograft Model of Non–Small Cell Lung Cancer. *J Nucl Med*. 2018;59:1686-1691.

9. Jagoda EM, Lang L, Bhadrasetty V, et al. Immuno-PET imaging of the hepatocyte growth factor receptor Met using the one-armed antibody Onartuzumab (MetMAb). *J Nucl Med*. 2012;53:1592-1600.

10. Pool M, Terwisscha van Scheltinga AGT, Kol A, Giesen D, de Vries EGE, Lub-de Hooge MN. 89Zr-Onartuzumab PET imaging of c-MET receptor dynamics. *Eur J Nucl Med Mol Imaging*. 2017;44:1328-1336.

11. Escorcia FE, Houghton JL, Abdel-atti D, et al. Theranostics ImmunoPET Predicts Response to Met-targeted Radioligand Therapy in Models of Pancreatic Cancer Resistant to Met Kinase Inhibitors. *Theranostics*. 2020;10:151-165.

12. Merchant M, Ma X, Maun HR, et al. Monovalent antibody design and mechanism of action of onartuzumab, a MET antagonist with anti-tumor activity as a therapeutic agent. *Proc Natl Acad Sci*. 2013;110:E2987-E2996.

13. Gherardi E, Birchmeier W, Birchmeier C, Woude G Vande. Targeting MET in cancer: Rationale and progress. *Nat Rev Cancer*. 2012;12:89-103.

14. Spigel DR, Edelman MJ, O'Byrne K, et al. Results From the Phase III Randomized Trial of Onartuzumab Plus Erlotinib Versus Erlotinib in Previously Treated Stage IIIB or IV Non-Small-Cell Lung Cancer: METLung. *J Clin Oncol*. 2017;35:412-420.

15. Patra M, Eichenberger LS, Fischer G, Holland JP. Photochemical conjugation and one-pot radiolabelling of antibodies for immuno-PET. *Angew Chemie Int Ed*. 2019;58:1928-1933.

16. Eichenberger LS, Patra M, Holland JP. Photoactive chelates for radiolabelling proteins. *Chem Commun*. 2019;55:2257-2260.

17. Patra M, Klingler S, Eichenberger LS, Holland J. Simultaneous Photoradiochemical Labelling of Antibodies for Immuno-PET. *iScience*. 2019;13:416-431.

18. Fay R, Gut M, Holland JP. Photoradiosynthesis of 68Ga-Labeled HBED-CC-Azepin-MetMAb for Immuno-PET of c-MET Receptors. *Bioconjug Chem*. 2019;30:1814-1820.

19. Gut M, Holland JP. Synthesis and Photochemical Studies on Gallium and Indium Complexes of DTPA-PEG3-ArN3 for Radiolabelling Antibodies. *Inorg Chem*. 2019;58:12302-12310.

20. Xiang H, Bender BC, Reyes AE, et al. Onartuzumab (MetMab): Using nonclinical pharmacokinetic and concentration-effect data to support clinical development. *Clin Cancer Res*. 2013;19:5068-5078.

21. Lindmo T, Boven E, Cuttitta F, Fedorko J, Bunn PA. Determination of the immunoreactive function of radiolabeled monoclonal antibodies by linear extrapolation to binding at infinite antigen excess. *J Immunol Methods*. 1984;72:77-89.

22. Fridman R, Benton G, Aranoutova I, Kleinman HK, Bonfil RD. Increased initiation and growth of tumor cell lines, cancer stem cells and biopsy material in mice using basement membrane matrix protein (Cultrex or Matrigel) co-injection. *Nat Protoc*. 2012;7:1138-1144.

23. Mattes JM. Limitations of the Lindmo method in determining immunoreactivity. *Int J Cancer*. 1995;61:286-288.

24. Junghans RP. Cruel antibody fictions! Cellular antigen enumeration by "saturation" binding. *Immunol Today*. 1999;20:401-406.

25. Konishi S, Hamacher K, Vallabhajosula S, et al. Determination of immunoreactive fraction of radiolabeled monoclonal antibodies: what is an appropriate method? *Cancer Biother Radiopharm*. 2004;19:706-15.

26. Gritsan NP, Platz MS. Kinetics, spectroscopy, and computational chemistry of arylnitrenes. *Chem Rev*. 2006;106:3844-3867.

27. Gritsan N, Platz M. Photochemistry of Azides : The Azide / Nitrene Interface. (Bräse S, Banert K, eds.). Wiley; 2010.

28. Borden WT, Gritsan NP, Hadad CM, Karney WL, Kemnitz CR, Platz MS. The interplay

of theory and experiment in the study of phenylnitrene. *Acc Chem Res*. 2000;33:765-771.

29. Platz MS. Comparison of Phenylcarbene and Phenylnitrene. *Acc Chem Res*. 1995;28:487-492.

30. Holland JP. Chemical Kinetics of Radiolabelling Reactions. *Chem Eur J*. 2018;24:16472-16483.

31. Richardson-Sanchez T, Tieu W, Gotsbacher MP, Telfer TJ, Codd R. Exploiting the biosynthetic machinery of: Streptomyces pilosus to engineer a water-soluble zirconium(IV) chelator. *Org Biomol Chem*. 2017;15:5719-5730.

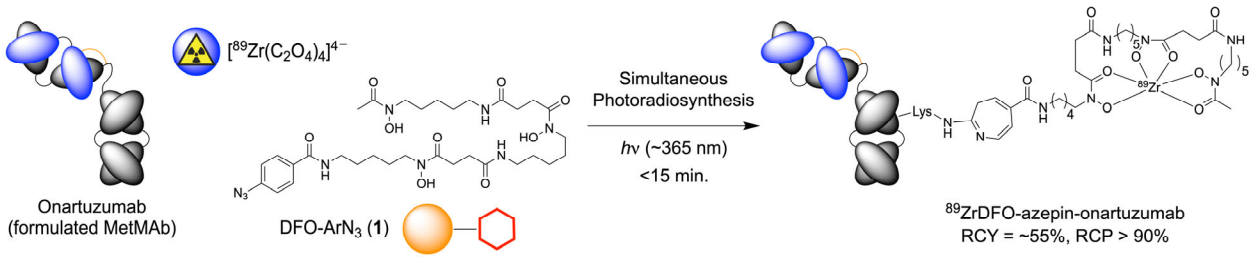

Figure 1. Multiple component photoradiosynthesis of monovalent (one-armed) ^{89}ZrDFO-azepin-onartuzumab starting from fully formulated MetMAb, the photoactive chelate DFO-ArN_3, and $[^{89}Zr(C_2O_4)_4]^{4-}$ (^{89}Zr-oxalate).

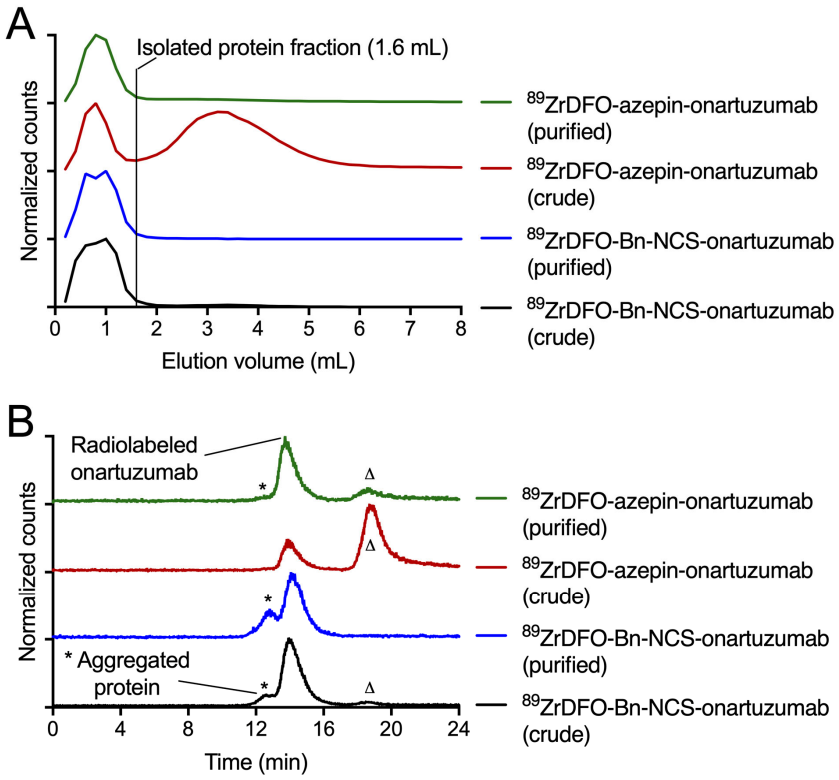

Figure 2. Chromatographic data on the radiosynthesis of ^{89}ZrDFO-azepin-onartuzumab and ^{89}ZrDFO-Bn-NCS-onartuzumab showing (A) elution profiles from analytical PD-10 size-exclusion columns, and (B) SEC-HPLC radiochromatograms, for the crude and purified samples of each radiotracer. 'Δ' indicates the retention time of small molecule impurities, '*' indicates the elution of high molecular weight protein aggregates. See Supplemental Figure 2 for radio-iTLC data.

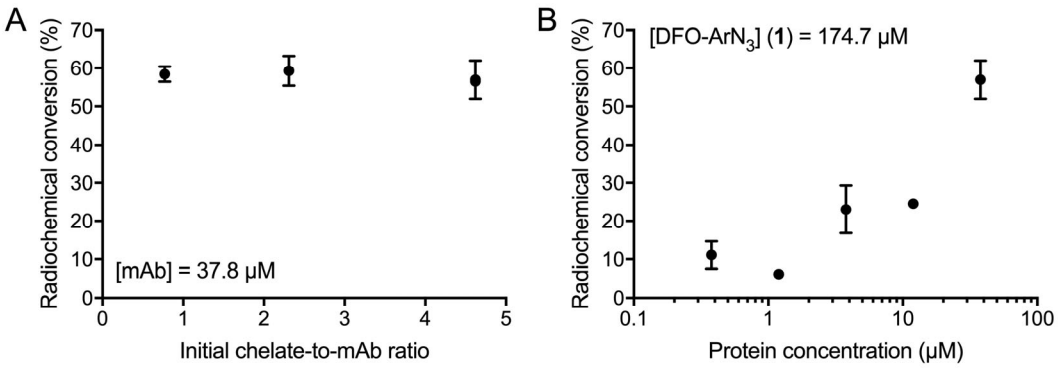

Figure 3. Radiochemical conversions (%) measured by SEC-HPLC methods for the optimization of the photoradiosynthesis of ^{89}ZrDFO-azepin-onartuzumab with, (A) varying initial chelate-to-mAb ratios (with a fixed protein concentration of 37.8 μM), and with (B) varying protein concentrations. See also Supplemental Table 1.

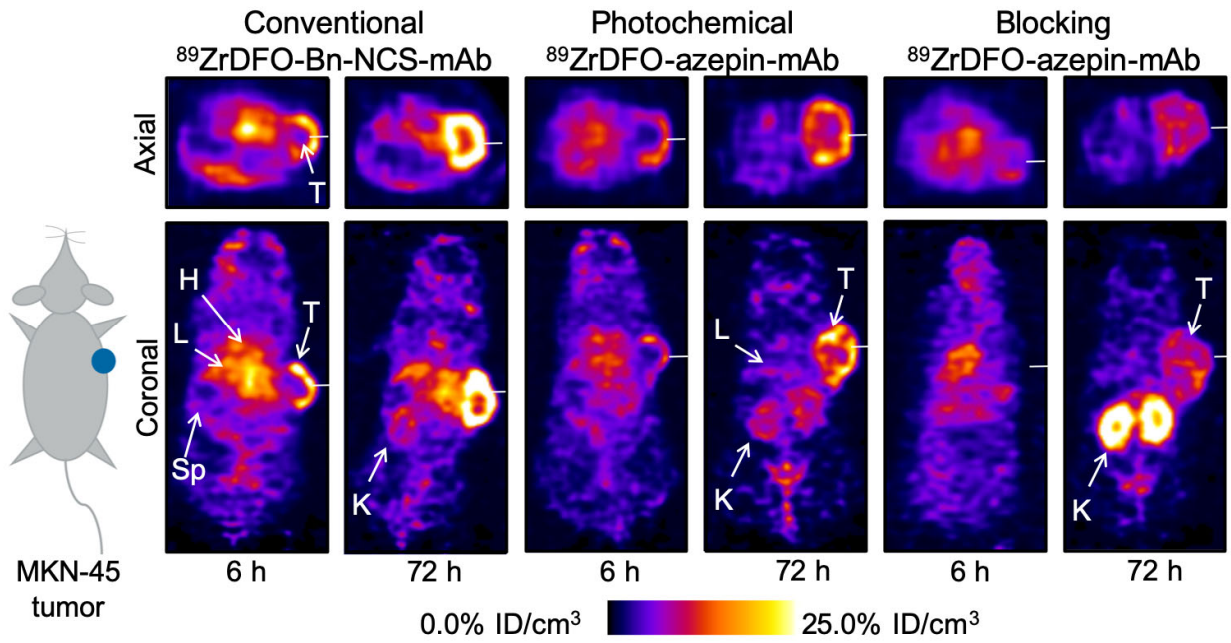

Figure 4. Temporal PET images recorded in athymic nude mice bearing MKN-45 tumors on the right flank for (left) ^{89}ZrDFO-Bn-NCS-onartuzumab, (middle) ^{89}ZrDFO-azepin-onartuzumab (normal group), and (right) ^{89}ZrDFO-azepin-onartuzumab (blocking group). T=tumor, H=heart, L=liver, Sp=spleen. Planar images are shown through the tumor center. See also Supplemental Figures 5 and 6.

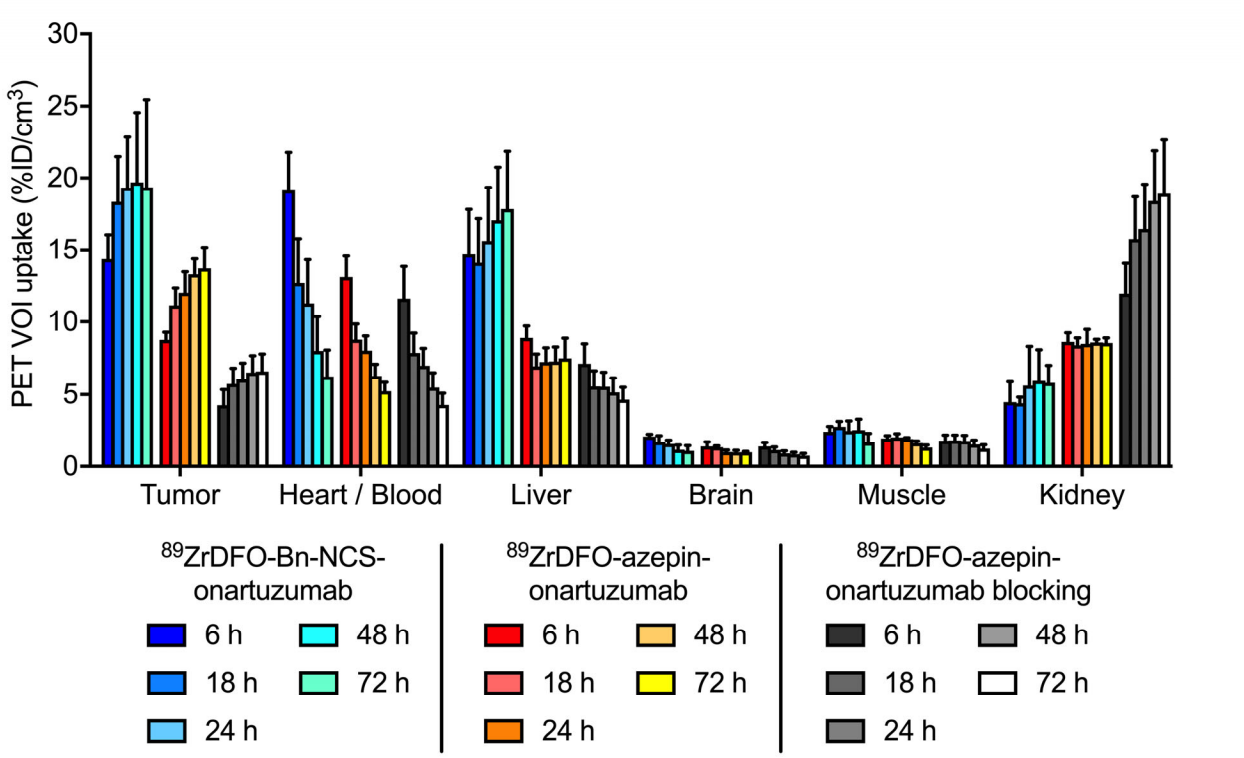

Figure 5. Time-activity bar chart showing the mean activity (%ID cm^{-3}) associated with different tissues *versus* time. ^{89}ZrDFO-Bn-NCS-onartuzumab (blue bars; *n*=4), ^{89}ZrDFO-azepin-onartuzumab (normal group; red-to-yellow bars; *n*=4), and ^{89}ZrDFO-azepin-onartuzumab (blocking group; grey-to-white bars; *n*=4). See also Supplemental Figure 7.

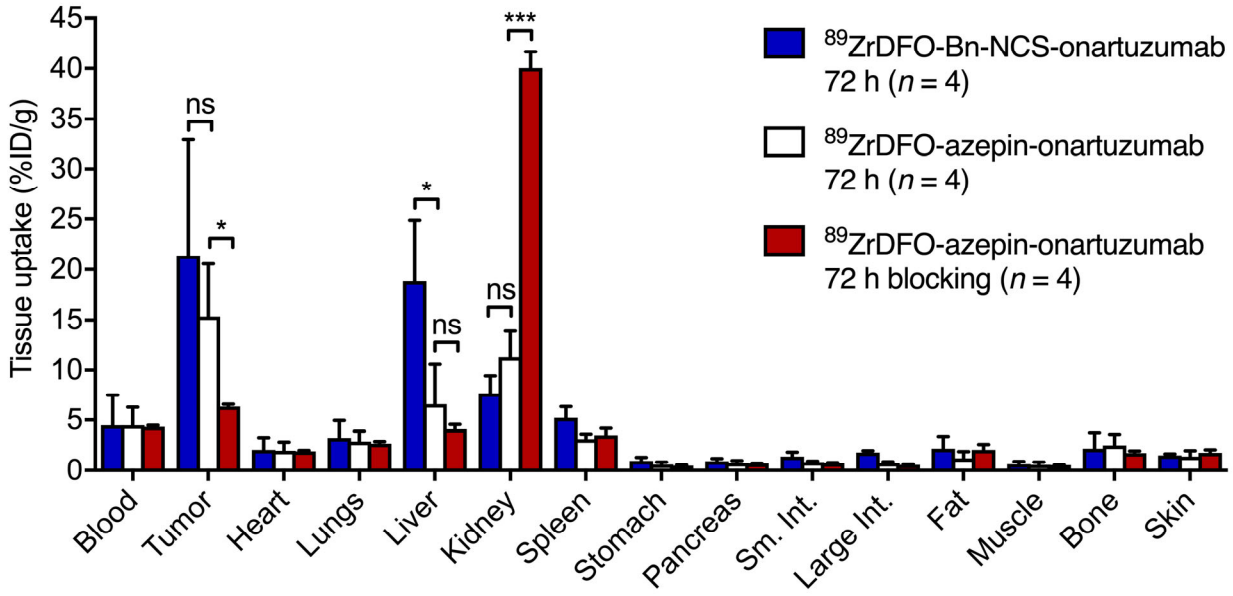

Figure 6. Bar chart showing *ex vivo* biodistribution data (%ID g^{-1}) for the uptake of ^{89}ZrDFO-Bn-NCS-onartuzumab (blue bars), ^{89}ZrDFO-azepin-onartuzumab (normal group, white bars), and ^{89}ZrDFO-azepin-onartuzumab (blocking group, red bars) in mice bearing MKN-45 tumors at 72h post-injection. Student's *t*-test: (ns) not significant, (*) *P*-value<0.05, (**) *P*-value<0.01, (***) *P*-value<0.001. See also Supplemental Figures 9 and 10.

Electronic Supporting Information (ESI)

Light-induced radiosynthesis of ^{89}ZrDFO-azepin-onartuzumab for imaging the hepatocyte growth factor receptor

Simon Klingler, Rachael Fay and Jason P. Holland*

University of Zurich, Department of Chemistry, Winterthurerstrasse 190, CH-8057, Zurich, Switzerland

*** Corresponding Author:**

Prof. Dr Jason P. Holland

Tel: +41.44.63.53.990

E-mail: jason.holland@chem.uzh.ch

Website: www.hollandlab.org

Table of Contents

General details

The synthesis and characterisation of DFO-ArN_3 was reported elsewhere.(*1*) Unless otherwise stated, all chemicals were of reagent grade and purchased from SigmaAldrich (St. Louis, MO), Merck (Darmstadt, Germany), Tokyo Chemical Industry (Eschborn, Germany), abcr (Karlsruhe, Germany) or CheMatech (Dijon, France). Water (>18.2 MΩ·cm at 25 ºC, Puranity TU 3 UV/UF, VWR International, Leuven, Belgium) was further purified by using Chelex resin to remove contaminant metal ions. Solvents for reactions were of reagent grade, and where necessary, were dried over molecular sieves. Evaporation of the solvents was performed under reduced pressure by using a rotary evaporator (Rotavapor R-300, Büchi Labortechnik AG, Flawil, Switzerland) at the specified temperature and pressure. Electronic absorption spectra were recorded using a Nanodrop^{TM} One^{C} Microvolume UV-Vis Spectrophotometer (ThermoFisher Scientific, supplied by Witec AG, Sursee, Switzerland). Protein concentration was determined in accordance with the manufacturers protocol.

Photochemistry

Photochemical conjugation experiments were performed in transparent glass vials at the specified concentrations. Unless otherwise stated, photochemical reactions were typically stirred gently by adding a small magnetic stir bar to the reaction vial and employing a slow stirring rate (< 1000 rpm) to avoid potential damage to the protein. Detail procedures and reaction times are indicated in the experimental section. Ultra-violet irradiations were performed by using a portable light-emitting diode (LED 365 nm). The LED intensity was adjusted using a digital UV-LED controller (Opsytec Dr. Gröbel GmbH, Ettlingen, Germany), where 100% corresponded to a power of approximately 263 mW at 365 nm. LED intensity was measured by using a S470C Thermal Power Sensor Head Volume Absorber, 0.25 – 10.6 µm, 0.1 mW – 5W, Ø15 mm. The temperature of all photochemical conjugation reactions was typically 23 ± 2 ºC (ambient conditions). An experimentally measured emission spectrum of the LED light source and a plot of the power *versus* digitally controlled LED intensity (as a percentage of maximum current) are shown in Supplemental Figures 1A and 1B, respectively. The LED source (365 nm) had a linear response with changing LED intensity with a peak emission at 364.5 nm and a FWHM of 9.1 nm.

Supplemental Figure 1. (A) Emission spectrum of the LED (365 nm), and (B) the measured power output (mW) *versus* the digitally controlled LED intensity (%).

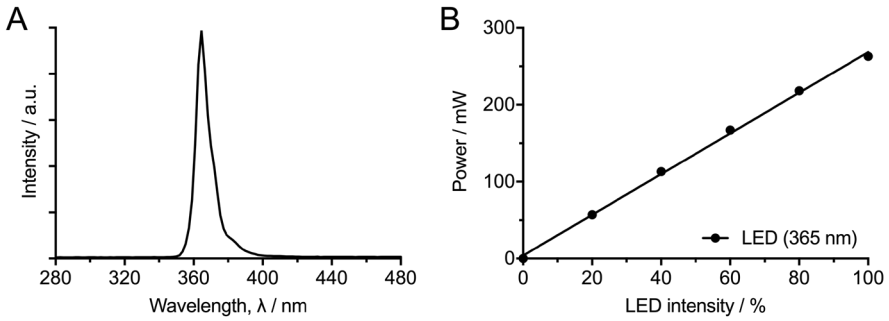

Radioactivity and radioactive measurements

All instruments for measuring radioactivity were calibrated and maintained in accordance with previously reported routine quality control procedures.(*2*) $[^{89}Zr][Zr(C_2O_4)_4]^{4-}$(aq.) was obtained as a solution in ~1.0 M oxalic acid from PerkinElmer (Boston, MA, manufactured by the BV Cyclotron VU, Amsterdam, The Netherlands) and was used without further purification. Radioactive reactions were monitored by using instant thin-layer chromatography (radio-iTLC). Glass-fibre iTLC plates impregnated with silica-gel (iTLC-SG, Agilent Technologies) were developed in using aqueous mobile phases containing DTPA (50 mM, pH7.1) and were analysed on a radio-TLC detector (SCAN-RAM, LabLogic Systems Ltd, Sheffield, United Kingdom). Radiochemical conversion (RCC) was determined by integrating the data obtained by the radio-TLC plate reader and determining both the percentage of radiolabelled product (R_f = 0.0) and 'free' ^{89}Zr (R_f = 1.0; present in the analyses as $[^{89}Zr][Zr(DTPA)]^-$). Integration and data analysis were performed by using the software Laura version 5.0.4.29 (LabLogic). Appropriate background and decay corrections were applied as necessary. Radiochemical purities (RCPs) of labelled protein samples were determined by size-exclusion chromatography (SEC) using two different columns and techniques. The first technique used an automated size-exclusion column (Bio-Rad Laboratories, ENrich SEC 70, 10 ± 2 µm, 10 mm ID x 300 mm) connected to a Rigol HPLC system (Contrec AG, Dietikon, Switzerland) equipped with a UV/visible detector (absorption measured at 220, 254 and 280 nm) as well as a radioactivity detector (FlowStar^2 LB 514, Berthold Technologies, Zug, Switzerland). Isocratic elution with phosphate buffered saline

(PBS, pH7.4) was used. The second method used a manual procedure involving size-exclusion column chromatography and a PD-10 desalting column (Sephadex G-25 resin, 85-260 µm, 14.5 mm ID x 50 mm, >30 kDa, GE Healthcare). For analytical procedures, PD-10 columns were eluted with PBS. A total of 40 x 200 µL fractions were collected up to a final elution volume of 8 mL. Note that the loading/dead-volume of the PD-10 columns is precisely 2.50 mL which was discarded prior to aliquot collection. For quantification of radioactivity, each fraction was measured on a gamma counter (HIDEX Automatic Gamma Counter, Hidex AMG, Turku, Finland) using an energy window between 480 – 558 keV for ^{89}Zr (511 keV emission) and a counting time of 30 s. Appropriate background and decay corrections were applied throughout. PD-10 SEC columns were also used for preparative purification and reformulation of radiolabelled products (in sterile PBS; pH7.4) by collecting a fraction of the eluate corresponding to the high molecular weight protein (>30 kDa fraction eluted in the range 0.0 mL to either 1.6 mL or 1.8 mL as indicated for each experiment).

Synthesis and chemical characterisation

Chemical synthesis and characterisation of DFO-ArN_3 and DFO-Bn-NCS-onartuzumab were performed in accordance with previously reported methods.(*1*,*3*) Note, the bioconjugation reaction using DFO-Bn-NCS,(*4*)(*5*) required pre-purification of the humanized, monovalent onartuzumab protein from the formulated solution of MetMAb by standard spin centrifugation methods.

^{89}Zr-radioactive stocks

A stock solution of [^{89}Zr][Zr(C_2O_4)$_4$]$^{4-}$ was prepared by adding ^{89}Zr radioactivity from the source (222.7 MBq, 140 µL in ~1.0 M aqueous oxalic acid) to an Eppendorf tube. The solution was neutralised and made slightly basic by the addition of aliquots of Na_2CO_3(aq.) (1.0 M stock solution, total volume of 180 µL added, final pH ~8.3 – 8.5, final volume ~320 µL, final activity = 215.8 MBq). Caution: Acid neutralisation with Na_2CO_3 releases CO_2(g) and care should be taken to ensure that no radioactivity escapes the microcentrifuge tube. After CO_2 evolution ceased, different reactions were performed at the same time using the same stock solutions.

Radiochemistry

Simultaneous photoradiosynthesis of [^{89}Zr]ZrDFO-azepin-onartuzumab

Simultaneous, one-pot photochemical conjugation and ^{89}Zr-radiolabelling reactions were performed in accordance with the following general procedure. A stock solution of DFO-ArN_3 was prepared by dissolving the purified white solid (**1**, 0.69 mg, 0.978 μmol) in H_2O (950 μL) and NaOH(aq.) (60 μL of a 0.1 M stock solution). The pH of the DFO-ArN_3 solution was adjusted to ~8 – 9 by the addition of HCl(aq.) (40 μL of a 0.1 M stock solution) and the final concentration of compound **1** was 0.932 mM. Note: DFO-ArN_3 (**1**) is sparingly soluble at high pH and starts to precipitate slowly when the pH decreases below ~9. Reactions were performed in optically transparent and colourless 2 mL glass vials equipped with small magnetic stirring bars.

Photoradiosynthesis of [^{89}Zr]ZrDFO-azepin-onartuzumab for animal experiments

To a glass vial containing H_2O (30 μL; chelex treated 18.2 MΩ.cm) was added an aliquot of the DFO-ArN_3 (**1**) stock solution (40 μL, 37.3 nmol). Then an aliquot of the neutralised stock solution of [^{89}Zr][Zr(C_2O_4)$_4$]$^{4-}$ was added (70 μL, 45.2 MBq). Then an aliquot of the stock solution of MetMAb was added (fully formulated, stock concentration = 60 mg/mL, MW(onartuzumab) = 99,180 Da, volume added = 10 μL, protein mass = 0.6 mg, protein moles = 6.05 nmol). The initial chelate-to-mAb ratio was 6.15 to 1. The reaction pH was measured and was between 7.9 – 8.3. The total reaction volume was ~150 μL giving a final [mAb] = 40.3 μM, and a final [DFO-ArN_3] = 248 μM. The reaction was stirred gently at room temperature and irradiated directly from the top of the vial for 10 min. Previous experiments using this reaction geometry confirmed that this was sufficient to affect ~100% photochemical reaction of the aryl azide group on compound **1**.(*1*) After the irradiation, reactions were then quenched by the addition of DTPA (10 μL, 50 mM, pH7) and aliquots of the crude reaction mixtures were purified by preparative PD-10-SEC (collecting the 0.0 – 1.6 mL high molecular weight fraction using sterile PBS as an eluent). Crude and pure mixtures were analysed by using analytical radio-ITLC, PD-10-SEC and SEC-HPLC. The isolated decay corrected radiochemical yield (RCY) of [^{89}Zr]ZrDFO-azepin-onartuzumab was 24.8% (*n* = 1) and the lower limit of the molar activity of

the product (estimated by assuming no protein losses) was ~1.5 MBq/nmol of protein, with an activity concentration of 3.87 MBq/mL. The radiochemical purity of the purified samples of [^{89}Zr]ZrDFO-azepin-onartuzumab was estimated to be ~90% (measured by SEC-HPLC).

Preparation of [^{89}Zr]ZrDFO-azepin-onartuzumab doses for injection

An aliquot of (2.463 MBq) of the purified and formulated sample of [^{89}Zr]ZrDFO-azepin-onartuzumab was added to a sterile vial and diluted with sterile PBS to a final volume of 1.1 mL. Syringes containing an average of 222 ± 15 µL were drawn with the average dose containing 0.471 ± 0.047 MBq (equivalent to 30.3 ± 0.31 µg of protein, 0.336 ± 0.031 nmol of protein).

For the competitive inhibition (blocking) experiments, a separate aliquot (2.410 MBq) of the purified and formulated sample of [^{89}Zr]ZrDFO-azepin-onartuzumab was added to a sterile vial. Then an aliquot of the stock solution of MetMAb (fully formulated; 60 mg/mL, 83 µL, 4.98 mg of protein) was added and the mixture was diluted with sterile PBS to a final volume of 1.1 mL. Syringes containing an average of ~208 ± 3 µL were drawn with the average dose containing 0.433 ± 0.011 MBq (equivalent to 971 ± 14 µg of protein, 9.79 ± 0.144 nmol of protein – a 29-fold increase in the administered protein mass for these blocking doses compared to the normal doses).

Classical radiosynthesis of [^{89}Zr]ZrDFO-Bn-NCS-onartuzumab

Radiosynthesis of [^{89}Zr]ZrDFO-Bn-NCS-onartuzumab for animal experiments

Conjugated DFO-Bn-NCS-onartuzumab was prepared as previously reported(*3*) using the standard protocol from Vosjan *et al*.(*4*) Radiolabelling with [^{89}Zr][Zr(C_2O_4)$_4$]$^{4-}$ was accomplished by using standard procedures.(*6*) Briefly, an aliquot of DFO-Bn-NCS-onartuzumab (65 µL formulated in saline, stock protein concentration = 3.84 mg/mL, pH7, protein mass = 0.250 mg, protein moles = 2.52 nmol) was added to an Eppendorf tube containing water (107 µL; chelex treated 18.2 MΩ.cm). Then an aliquot of the neutralised stock solution of [^{89}Zr][Zr(C_2O_4)$_4$]$^{4-}$ was added (60 µL, 39.4 MBq,). The reaction pH was measured and was between 7.9 – 8.3. The total reaction volume was ~232 µL giving a final [mAb] = 10.9 µM. The reaction was incubated at room temperature for ~45 min. and was then quenched by the addition of DTPA (10 µL, 50 mM, pH7). Aliquots of the crude reaction mixtures were purified by

preparative PD-10-SEC (collecting the 0.0 – 1.6 mL high molecular weight fraction using sterile PBS as an eluent). Crude and pure mixtures were analysed by using analytical radio-ITLC, PD-10-SEC and SEC-HPLC. The isolated decay corrected radiochemical yield (RCY) of [^{89}Zr]ZrDFO-azepin-onartuzumab was >97% (n = 1) and the lower limit of the molar activity of the product (estimated by assuming no protein losses) was ~14.0 MBq/nmol of protein, with an activity concentration of 19.0 MBq/mL. The radiochemical purity of the purified samples of [^{89}Zr]ZrDFO-azepin-onartuzumab was estimated to be >97% (measured by SEC-HPLC).

Preparation of [^{89}Zr]ZrDFO-Bn-NCS-onartuzumab doses for injection

An aliquot of (2.463 MBq) of the purified and formulated sample of [^{89}Zr]ZrDFO-Bn-NCS-onartuzumab was added to a sterile vial and diluted with sterile PBS to a final volume of 1.1 mL. Syringes containing an average of 210 ± 2 µL were drawn with the average dose containing 0.571 ± 0.016 MBq (equivalent to 4.04 ± 0.15 µg of protein, 0.041 ± 0.001 nmol of protein).

Supplemental Figure 2. Radio-iTLC chromatograms recorded during the production of [^{89}Zr]ZrDFO-Bn-NCS-onartuzumab and [^{89}Zr]ZrDFO-azepin-onartuzumab for use in animal studies.

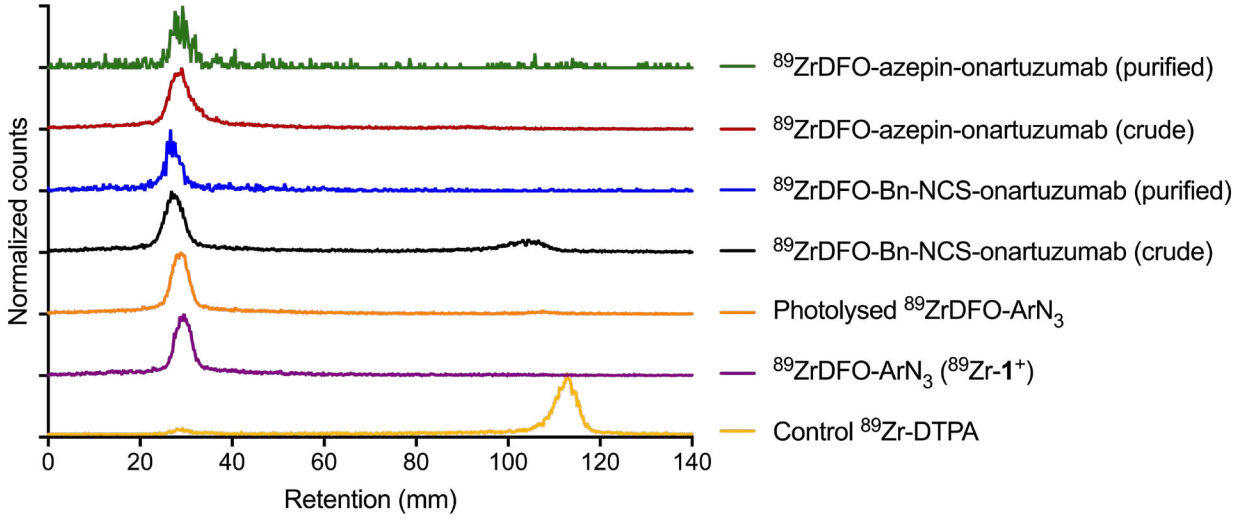

Optimisation of the photoradiosynthesis of [^{89}Zr]ZrDFO-azepin-onartuzumab

Effect of changing the initial chelate-to-mAb ratio and protein concentration

Experiments were performed to measure the effect of altering the initial chelate-to-mAb ratio on the efficiency of the simultaneous, one-pot photochemical conjugation and ^{89}Zr-radiolabelling of onartuzumab (using fully formulated MetMAb). Photoradiosynthesis experiments were set-up in an identical fashion to the reaction used to produce the dose for use in animal experiments. Unless otherwise stated, all reactions were stirred gently and were performed in triplicate using independent replicates. In all cases, the final reaction volume was 160 µL. All reactions were irradiated using 365 nm light for 10 min at ambient temperature. The protein concentration of the stock solution of formulated MetMAb was 60 mg/mL. The [DFO-ArN_3] was 0.932 mM. The same neutralised stock solution of [^{89}Zr][Zr(C_2O_4)$_4$]$^{4-}$ was used throughout and all experiments were performed on the same day to limit the effects of changes in molar activity. Full details are given in Supplemental Table 1.

Supplemental Table 1. Reaction parameters used during the optimisation of the one-pot photoradiosynthesis of [^{89}Zr]ZrDFO-azepin-onartuzumab starting from formulated MetMAb.

Parameter	Reactions A, B and C	Reactions D, E and F	Reactions G, H and I	Reaction J (not stirred)[b]	Reactions K and L	Reactions M and N	Reactions O and P	Reactions Q and R
Vol. MetMAb stock / µL	10	10	10	10	3.2	1	0.32	0.1
n(mAb) / nmol	6.05	6.05	6.05	6.05	1.91	0.605	0.19	0.06
Vol. DFO-ArN_3 stock / µL	30	15	5	30	30	30	30	30
n(DFO-ArN_3) / nmol	27.95	13.97	4.66	27.95	27.95	27.95	27.95	27.95
Initial chelate-to-mAb ratio	4.62	2.31	0.77	4.62	14.6	46.2	146.1	461.9
Radiochemical conversion (RCC) / % measured from SEC-HPLC for each replicate	A = 57.1 B = 61.9 C = 51.9	D = 63.8 E = 56.0 F = 58.2	G = 59.6 H = 56.1 I = 59.5	J = 56.5	K = 23.6 L = 25.6	M = 27.5 N = 18.7	O = 6.7 P = 5.6	Q = 13.7 R = 8.6
Average RCC ± one standard deviation (s.d.) / %	56.9 ± 4.1	59.3 ± 3.3	58.4 ± 1.6	56.5	24.6 ± 1.4	23.1 ± 6.2	6.1 ± 0.8	11.1 ± 3.6
Isolated decay corrected radiochemical yield (RCY) / %[a]	41.2 ± 10.6	33.7 ± 5.8	34.9 ± 10.4	Not determined	Not determined	Not determined	Not determined	Not determined
Average radiochemical purity (RCP) /% of the purified samples measured by SEC-HPLC	91.6 ± 0.6	91.3 ± 1.8	90.7 ± 2.3	Not determined	Not determined	Not determined	Not determined	Not determined

[a] RCY determined after isolation using preparative PD-10 SEC. [b] $n = 1$ replicate.

Stability studies

The stability of [^{89}Zr]ZrDFO-azepin-onartuzumab and [^{89}Zr]ZrDFO-Bn-NCS-onartuzumab with respect to change in radiochemical purity due to loss of radioactivity from the protein fraction was investigated *in vitro* by incubation in human serum. Aliquots (80 µL) of the purified and formulated radiotracers were added to a solution of human serum (320 µL) giving a total reaction volume of 400 µL. Solutions were incubated at 37 ºC and samples were withdrawn at various time points up to 48 h for analysis by SEC-HPLC measurements. The stability was monitored by quantifying the radioactivity associated with intact [^{89}Zr]ZrDFO-azepin-onartuzumab from integration of the decay corrected and baseline corrected SEC-HPLC radioactive chromatograms.

Supplemental Figure 3. Radioactive SEC-HPLC chromatograms recorded from samples [^{89}Zr]ZrDFO-Bn-NCS-onartuzumab (blue) and [^{89}Zr]ZrDFO-azepin-onartuzumab (green) incubated in human serum at 37 ºC for up to 48 h.

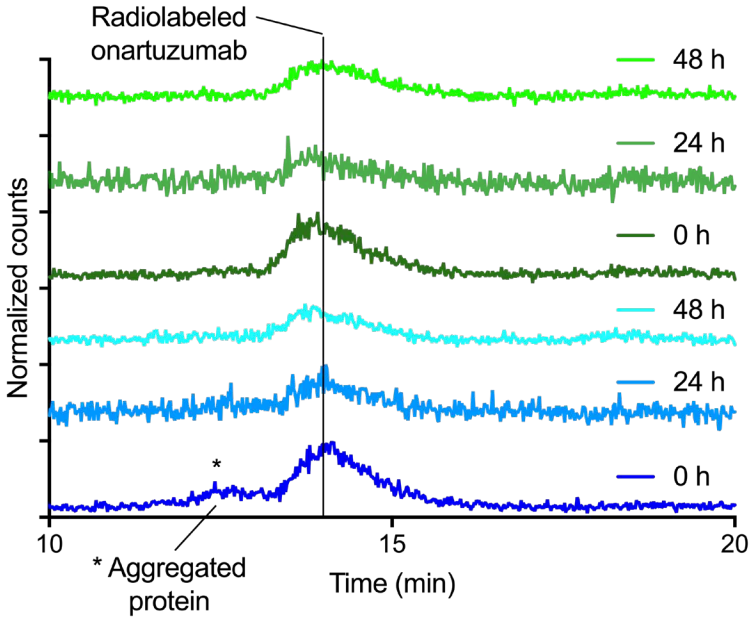

[^{89}Zr]ZrDFO-Bn-NCS-trastuzumab (blue)

[^{89}Zr]ZrDFO-azepin-trastuzumab (green)

Cell culture

For cell binding assays, the human gastric cancer cell line MKN-45 (c-MET positive and overexpressing, Leibniz Institute DSMZ-German collection of Microorganisms and Cell cultures [ACC 409]) was used. Cells were cultured at 37 °C in a humidified 5% CO_2 atmosphere. MKN-45 cells were cultured in RPMI-1640 (without phenol-red). The media was supplemented with fetal bovine serum (FBS, 10% (v/v), ThermoFisher Scientific) and penicillin/streptomycin (P/S, 1% (v/v) of penicillin 10000 U/mL and streptomycin 10 mg/mL). Cells were grown by serial passage and were harvested using trypsin-EDTA solution (0.025%). Cells were pelleted (100 g, 5 min) and resuspended in media before sequential passaging.

Cell binding assays (immunoreactivity)

Immunoreactivity was determined using a procedure adapted from Lindmo *et al*.(*7*) Briefly, MKN-45 cells were harvested and collected by centrifugation (100 g, 5 min). Two concentration series of 1:2 dilutions (in triplicate) were prepared in RPMI media. To one series, aliquots of purified [^{89}Zr]ZrDFO-azepin-MetMAb (~ 5 ng, ~ 335 Bq, 100 µL PBS) were added, and to the other, aliquots of purified [^{89}Zr]ZrDFO-Bn-NCS-MetMAb (~ 5 ng, ~ 3442 Bq, 100 µL PBS) were added to each cell concentration. To determine the extent of non-specific binding a fourth concentration series of the highest three concentrations was prepared and an ~35,000-fold excess of non-functionalised MetMAb (3 µL, 60 mg/mL, 0.18 mg) was added 30 min. before the addition of the radiotracer. Three samples of control radiotracers were also prepared to serve as standards for total activity added in the vials for each series. Vials were shaken gently at 400 rpm at 37 °C in a thermomixer for 4 h to ensure the cells remained in suspension. The cells were then pelleted by centrifugation (2000 rpm, 4 °C, 4 min.), the media was removed and the cells were washed twice with ice cold PBS with re-pelleting and removal of PBS between each wash. Cell associated radioactivity of the washed pellet was measured by using a Hidex gamma counter. The immunoreactive fraction was determined as the reciprocal y-intercept from the Lindmo transformation.

Supplemental Figure 4. Measurement of the immunoreactive fraction of [^{89}Zr]ZrDFO-azepin-onartuzumab (blue) and [^{89}Zr]ZrDFO-Bn-NCS-onartuzumab (black). (A) Saturation binding plot. (B) Lindmo plot.[a]

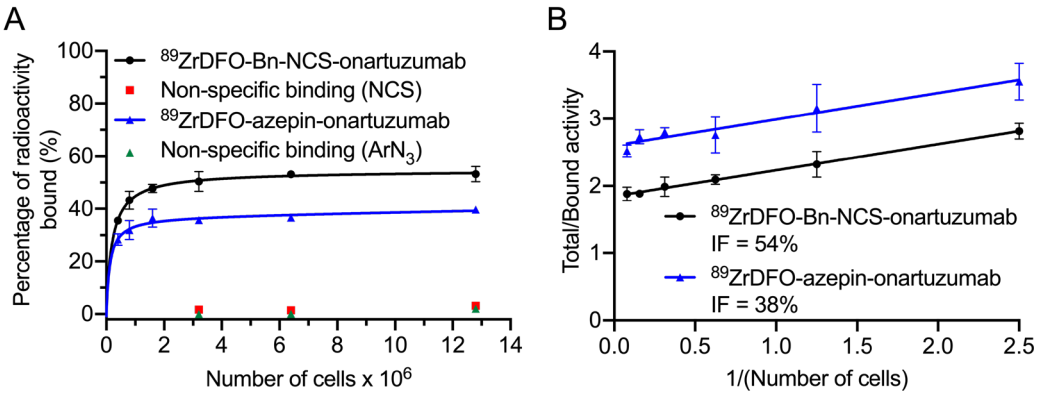

[a] Data account for differences in radiochemical purity.

Animals and xenograft models

All experiments involving mice were conducted in accordance with an animal experimentation licence approved by the Zurich Canton Veterinary Office, Switzerland (Jason P. Holland). Experimental procedures also complied with guidelines issued in the *Guide for the Care and Use of Laboratory Animals.*(*8*) Female athymic nude mice (Crl:NU(NCr)-*Foxn1*^{nu}, 20 – 25 g, 4 – 8 weeks old) were obtained from Charles River Laboratories Inc. (Freiburg im Breisgau, Germany), and were allowed to acclimatise at the University of Zurich Laboratory of Animal Science vivarium for at least 1 week prior to implanting tumour cells. Mice were provided with food and water *ad libitum*. Tumours were induced on the right shoulder or flank by sub-cutaneous (s.c.) injection of approx. 2.5 × 10^6 cells. The cells were injected in a 200 µL suspension of a 1:1 v/v mixture of PBS and reconstituted basement membrane (Corning® Matrigel® Basement Membrane Matrix, obtained from VWR International).(*9*) Tumours developed after a period of between 7 – 14 days. Tumour volume (V / mm^3) was estimated by external Vernier calliper measurements of the longest axis, a / mm, and the axis perpendicular to the longest axis, b / mm. The tumours were assumed to be spheroidal and the volume was calculated in accordance with Equation S1.

$$V = \frac{4\pi}{3} \cdot \left(\frac{a}{2}\right)^2 \cdot \left(\frac{b}{2}\right) \quad \text{(Equation S1)}$$

Small-animal PET imaging

All mice injected with cancer cells developed tumours and the average volume of the MKN-45 tumours was 577 ± 424 mm^3 (n = 12 mice; volume range = 135 – 1323 mm^3). Mice were randomised before the study. The tail of each mouse was warmed gently using a warm water bath immediately before administering [^{89}Zr]ZrDFO-azepin-onartuzumab (normal group n = 4 mice / group, where each dose contained activity = 0.471 ± 0.047 MBq, equivalent to 30.3 ± 0.31 μg of protein, 0.336 ± 0.031 nmol of protein, in 222 ± 15 μL sterile PBS) *via* intravenous (i.v.) tail-vein injection (t = 0 h). Competitive inhibition studies were also performed to investigate the specificity and biological activity of the radiotracer *in vivo* (blocking group: n = 4 mice / group, where each dose contained activity = 0.433 ± 0.011 MBq, equivalent to 971 ± 14 μg of protein, 9.79 ± 0.144 nmol of protein, in 208 ± 3 μL sterile PBS). For comparison with standard conjugation and radiolabelling chemistry, PET imaging was also performed on a group of mice administered with [^{89}Zr]ZrDFO-Bn-NCS-onartuzumab (normal group n = 4 mice / group, where each dose contained activity 0.571 ± 0.016 MBq, equivalent to 4.04 ± 0.15 μg of protein, 0.041 ± 0.001 nmol of protein, in 210 ± 2 μL sterile PBS). Full details on radioactive dose preparation are given in the Radiochemistry section above.

PET imaging experiments were conducted on a Genesis G4 PET/X-ray scanner (Sofie Biosciences, Culver City, CA).(*10*) Approximately 5 minutes prior to recording each PET image, mice were anesthetised by inhalation of between 2 – 4% isoflurane (Attane™, Piramal Enterprises Ltd, India, supplied by Provet AG, Lyssach, Switzerland)/oxygen gas mixture and placed on the scanner bed in the prone position. PET images were recorded at various time-points between 0 h and 72 h post-administration of the radiotracer. During image acquisition, the respiration rate of the animal was monitored *via* live video feed and anaesthesia was maintained by an experience animal experimenter by controlling the isoflurane dose between 1.5 – 2.0%. List-mode data were acquired for 10 min. using a γ-ray energy window of 150–650 keV, and a

coincidence timing window of 20 ns. Images were reconstructed by iterative ordered subset maximum expectation (OSEM; 60 iterations) protocols. The reported reconstructed spatial resolution is 2.4 μL at the centre of the field-of-view (FOV). Image data were normalised to correct for non-uniformity of response of the PET, attenuation, random events, dead-time count losses, positron branching ratio, and physical decay to the time of injection, but no scatter or partial-volume averaging correction was applied. An empirically determined system calibration factor (in units of [Bq/voxel]/[MBq/g] or [Bq/cm^3]/[MBq/g]) for mice was used to convert voxel count rates to activity concentrations. The resulting image data were normalised to the administered activity to parameterise images in terms of %ID cm^{-3} (equivalent to units of %ID/g assuming a tissue density of unity). Images were analysed by using VivoQuant^{TM} 3.5 patch 2 software (InviCRO, Boston, MA). For image quantification and measurements of time-activity curves (TACs), 3-dimensional volumes-of-interest (VOIs) were drawn manually to determine the maximum and mean accumulation of radioactivity (in units of %ID cm^{-3} and decay corrected to the time of injection) in various tissues. Where appropriate, data were also converted into mean standardised uptake values (SUV_{mean}).

Biodistribution studies

Biodistribution studies were conducted after the final imaging time point to evaluate the radiotracer uptake in tumour-bearing mice. Animals (n = 4 mice / group) were anaesthetised individually by isoflurane and euthanised by isoflurane asphyxiation followed by terminal exsanguination. Note: one mouse was excluded from the analysis of the data from the normal group (*vide supra*). A total of 15 tissues (including the tumour) were removed, rinsed in water, dried in air for approx. 2 min., weighed and counted on a calibrated gamma counter for accumulation of activity. The mass of radiotracer formulation injected into each animal was measured and used to determine the total number of counts per minute (cpm) injected into each mouse by comparison to a standard syringe of known activity and mass. Count data were background- and decay-corrected, and the tissue uptake for each sample (determined in units of percentage injected dose per gram [%ID g^{-1}]) was calculated by normalisation to the total amount of activity injected for each individual animal. For comparison purposes, data are also presented in terms of SUV.

Effective half-life, $t_{1/2}$(eff)

The effective half-lives $t_{1/2}$(eff) of [^{89}Zr]ZrDFO-azepin-onartuzumab and [^{89}Zr]ZrDFO-Bn-NCS-onartuzumab were measured in the same athymic nude mice used for small-animal PET imaging and end time point biodistribution. Total internal radioactivity was measured as a function of time by using a dose calibrator.

Statistical analysis

Where appropriate, data were analysed by the unpaired, two-tailed Student's *t*-test. Differences at the 95% confidence level (*P*-value <0.05) were considered to be statistically significant. Data analysis was performed using Microsoft Excel for MAC (version 16.16.10) and GraphPad Prism 7 for MAC OS X (version 7.0e).

PET imaging results

Supplemental Figure 5. Temporal PET images recorded in athymic nude mice bearing MKN-45 tumours on the right flank at time points between 0 h to 72 post-administration of (top) [^{89}Zr]ZrDFO-Bn-NCS-onartuzumab, (middle) [^{89}Zr]ZrDFO-azepin-onartuzumab (normal group), and (bottom) [^{89}Zr]ZrDFO-azepin-onartuzumab (blocking group). T = tumour, H = heart, L = liver, Sp = spleen. Coronal and axial planes are through the tumour centre.

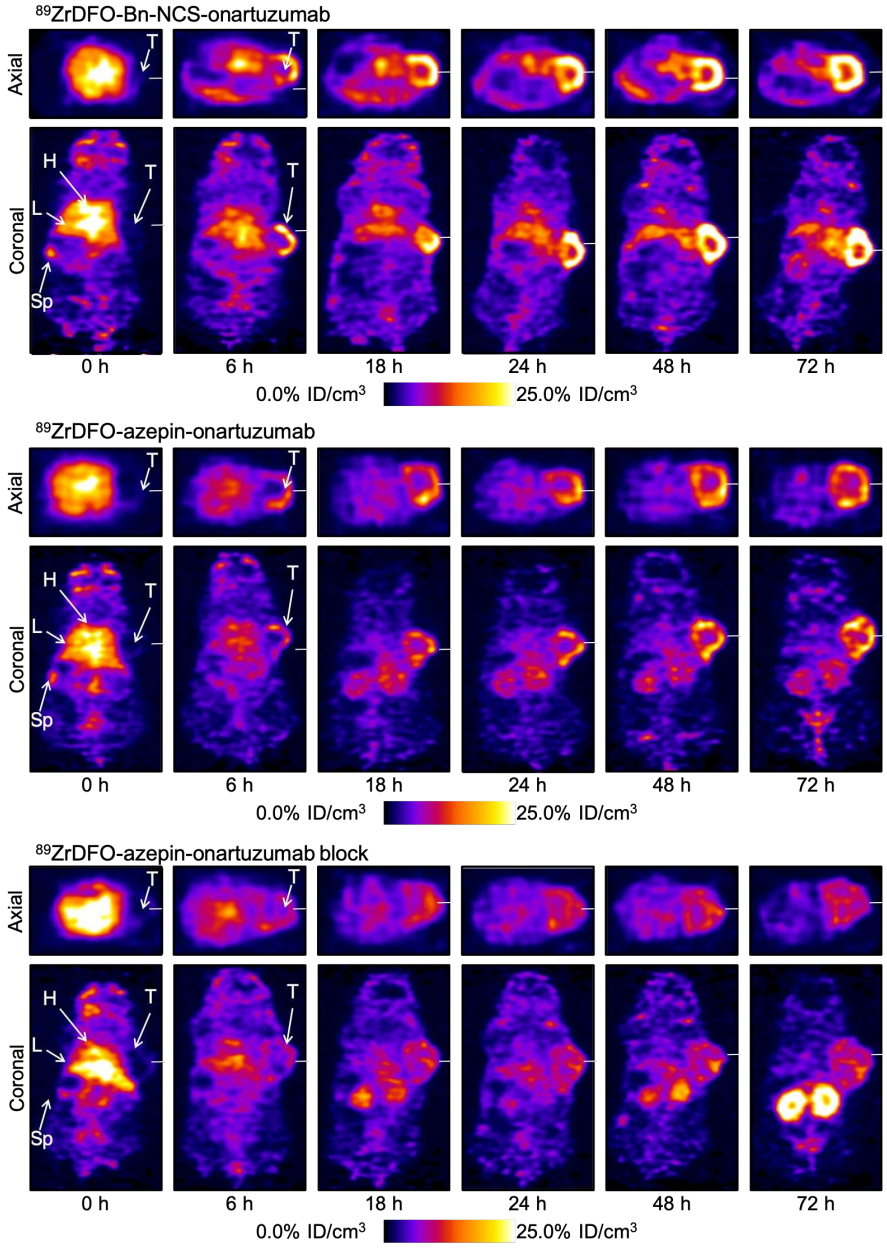

Supplemental Figure 6. Maximum intensity projection (MIP) PET images recorded in athymic nude mice bearing MKN-45 tumours on the right flank at time points between 0 h to 72 post-administration of (top) [^{89}Zr]ZrDFO-Bn-NCS-onartuzumab, (middle) [^{89}Zr]ZrDFO-azepin-onartuzumab (normal group), and (bottom) [^{89}Zr]ZrDFO-azepin-onartuzumab (blocking group). T = tumour, H = heart, L = liver, Sp = spleen, B = bladder, K = kidney.

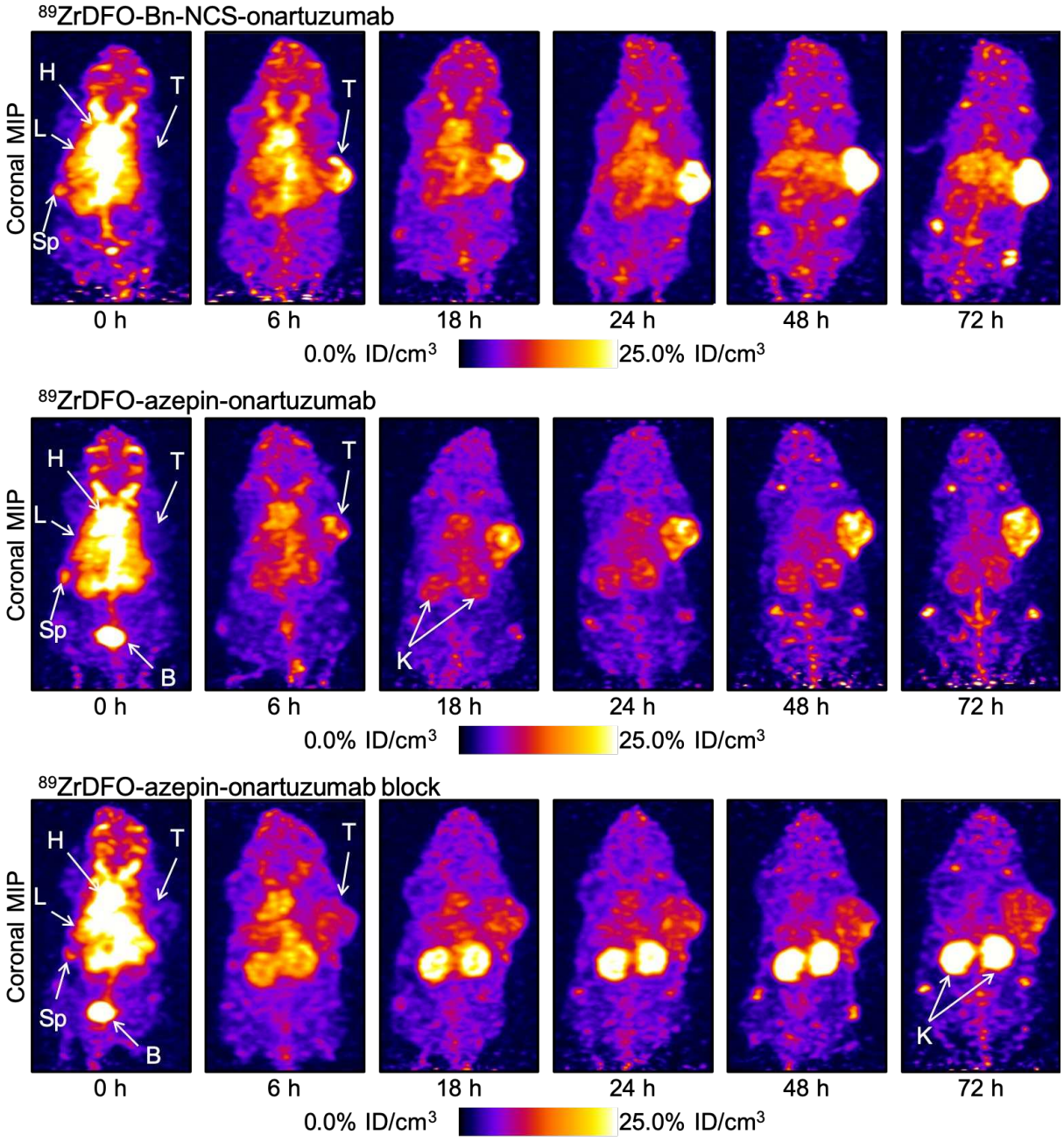

Supplemental Figure 7. Time-activity bar chart showing the activity associated with different tissues (volumes-of-interest, VOI) *versus* time (from 0 to 72 h post-administration). Data presented are based on quantification of the PET images (in units of %ID cm^{-1}) for [^{89}Zr]ZrDFO-Bn-NCS-onartuzumab (blue bars), [^{89}Zr]ZrDFO-azepin-onartuzumab (normal group; red-to-yellow bars), and [^{89}Zr]ZrDFO-azepin-onartuzumab (blocking group; black-to-white bars).

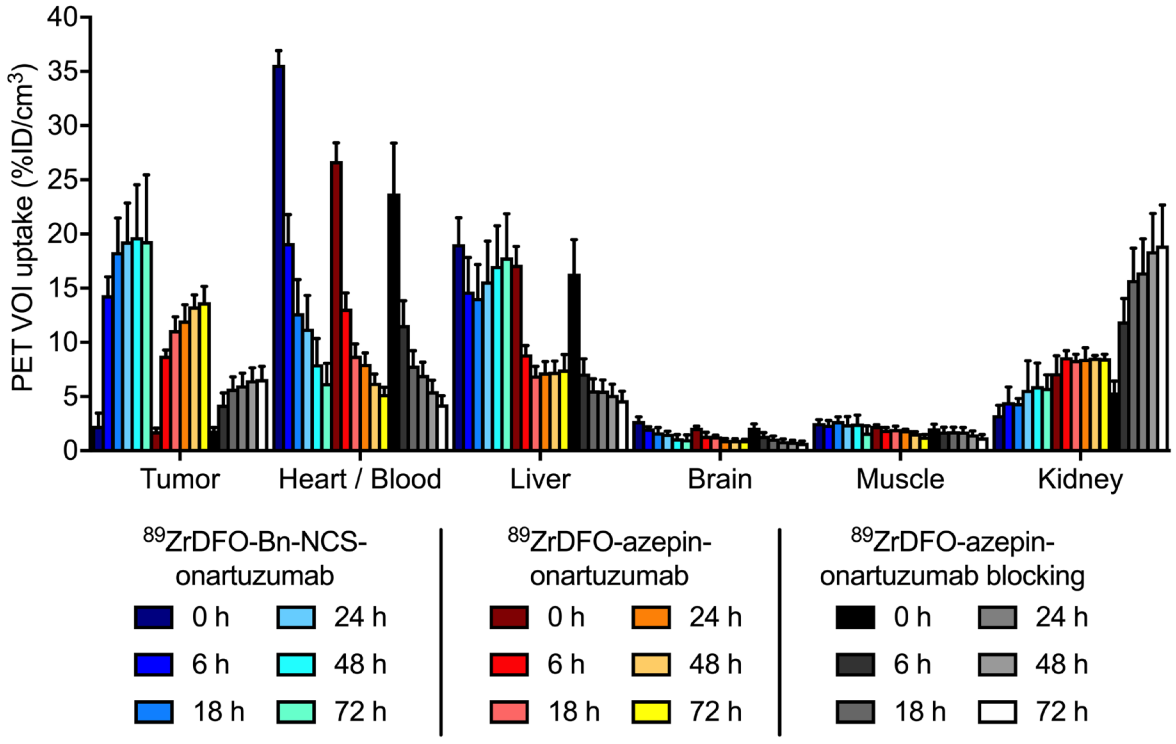

Supplemental Figure 8. Plot of the measured activity retained in each mouse *versus* time.[a] Data were used to estimate the effective and biological half-lives of [^{89}Zr]ZrDFO-Bn-NCS-onartuzumab and [^{89}Zr]ZrDFO-azepin-onartuzumab.

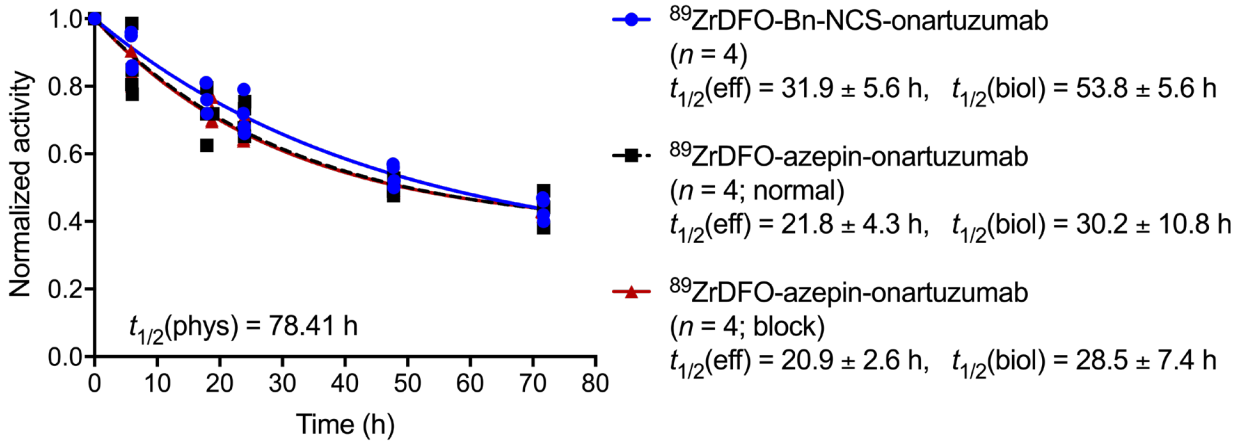

[a] Data account for differences in radiochemical purity.

Biodistribution data

Supplemental Figure 9. Bar chart showing *ex vivo* biodistribution data (SUV) for the uptake of [^{89}Zr]ZrDFO-Bn-NCS-onartuzumab (blue bars), [^{89}Zr]ZrDFO-azepin-onartuzumab (normal group, white bars), and [^{89}Zr]ZrDFO-azepin-onartuzumab (blocking group, red bars) in mice bearing MKN-45 tumours. Data were recorded after the final imaging time point at 72 h post-injection. Student's *t*-test: (ns) not significant, (*) *P*-value < 0.05, (**) *P*-value < 0.01, (***) *P*-value < 0.001.

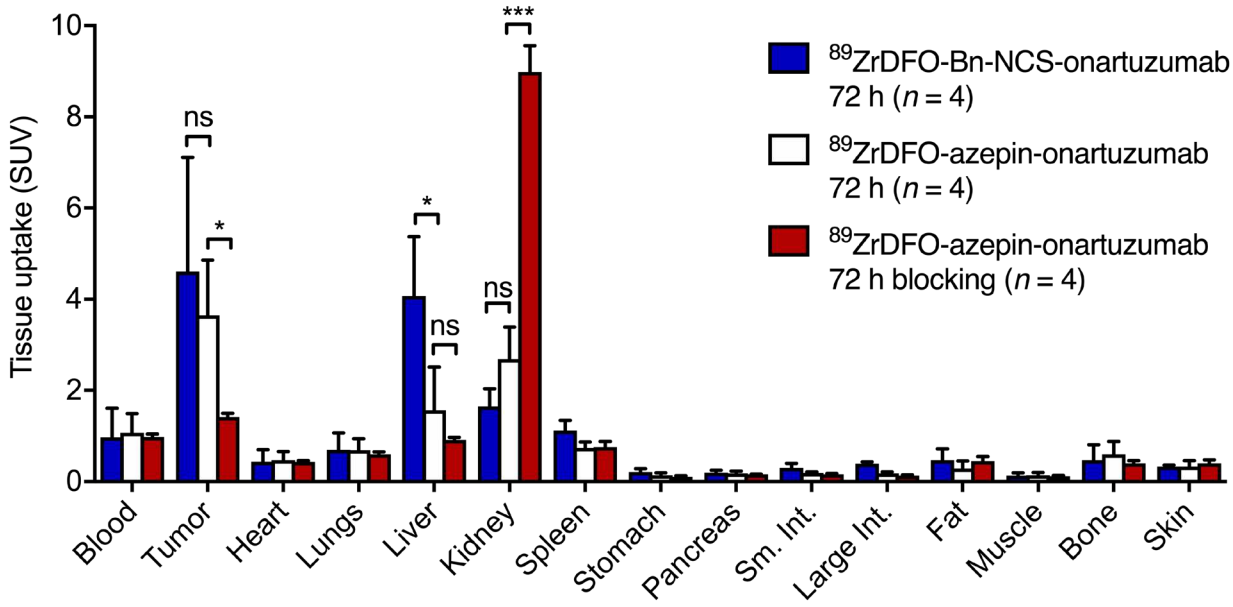

Supplemental Figure 10. Bar chart showing tumour-to-tissue contrast ratio calculated from the *ex vivo* biodistribution data (recorded at 72 h post-administration in units of %ID g^{-1}) for the uptake of [^{89}Zr]ZrDFO-Bn-NCS-onartuzumab (blue bars), [^{89}Zr]ZrDFO-azepin-onartuzumab (normal group, white bars), and [^{89}Zr]ZrDFO-azepin-onartuzumab (blocking group, red bars) in mice bearing MKN-45 tumours.

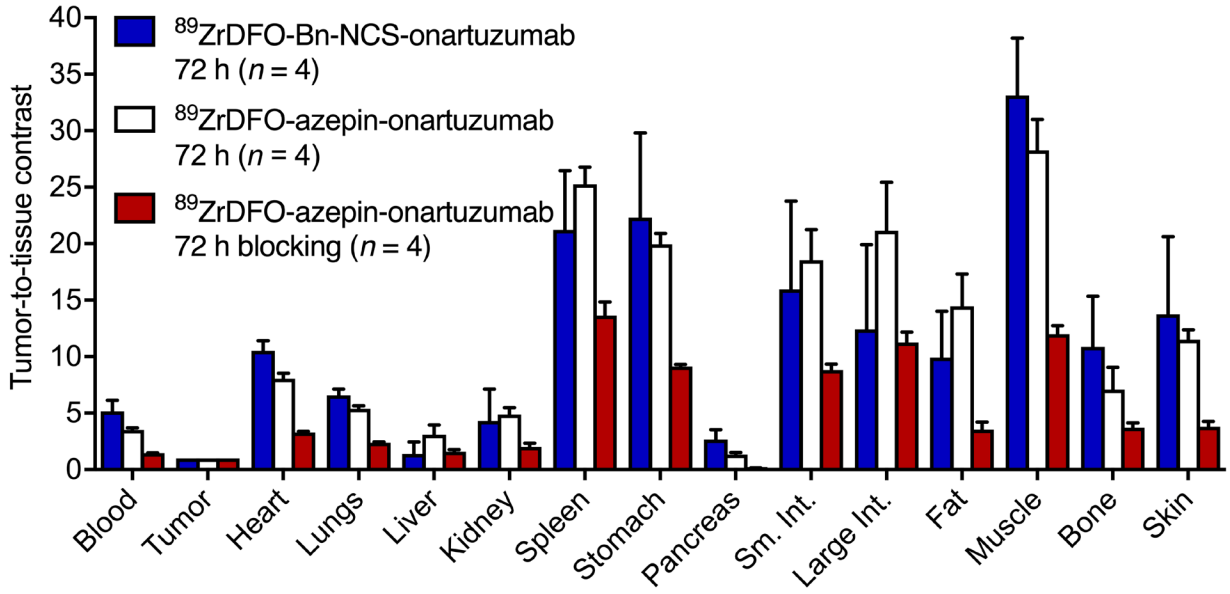

Supplemental Table 2. Ex vivo biodistribution data measured at 72 h after i.v. administration of ^{89}ZrDFO-azepin-onartuzumab (normal and blocking groups) and ^{89}ZrDFO-Bn-NCS-onartuzumab in female athymic nude mice bearing subcutaneous MKN-45 tumors. [a] Uptake data are expressed as the mean %ID g^{-1} ± one standard deviation (S.D.). [b] Errors for the tumor-to-tissue ratios are calculated as the standard deviations based on ratios from dependent pairs.

	^{89}ZrDFO-azepin-onartuzumab (normal group, n = 4)		^{89}ZrDFO-azepin-onartuzumab (blocking group, n = 4)		^{89}ZrDFO-Bn-NCS-onartuzumab (control group, n = 4)	
Tissue	Uptake / %ID g^{-1} ± S.D.[a]	Tumor-to-tissue contrast ratio ± S.D.[b]	Uptake / %ID g^{-1} ± S.D.[a]	Tumor-to-tissue contrast ratio ± S.D.[b]	Uptake / %ID g^{-1} ± S.D.[a]	Tumor-to-tissue contrast ratio ± S.D.[b]
Blood	4.49 ± 1.79	3.53 ± 0.36	4.35 ± 0.27	1.46 ± 0.08	4.50 ± 2.98	5.15 ± 0.99
Tumor	15.37 ± 5.21	1.00	6.34 ± 0.47	1.00	21.38 ± 11.57	1.00
Heart	1.98 ± 0.83	8.05 ± 0.97	1.92 ± 0.15	3.30 ± 0.18	2.05 ± 1.20	10.52 ± 0.91
Lungs	2.88 ± 1.02	5.39 ± 0.54	2.69 ± 0.36	2.38 ± 0.17	3.23 ± 1.72	6.59 ± 0.55
Liver	6.56 ± 4.03	3.11 ± 1.72	4.12 ± 0.94	1.60 ± 0.36	18.84 ± 6.03	1.38 ± 1.07
Spleen	3.10 ± 0.50	4.87 ± 1.23	3.49 ± 1.42	2.02 ± 0.66	5.22 ± 1.10	4.34 ± 2.79
Stomach	0.61 ± 0.23	25.25 ± 3.07	0.48 ± 0.10	13.63 ± 2.45	0.96 ± 0.33	21.22 ± 5.24
Pancreas	0.76 ± 0.21	19.95 ± 1.93	0.69 ± 0.04	9.13 ± 0.40	0.92 ± 0.25	22.31 ± 7.50
Kidney	11.28 ± 2.62	1.35 ± 0.36	40.05 ± 3.27	0.16 ± 0.01	7.64 ± 1.80	2.66 ± 0.89
Sm. Int.	0.82 ± 0.10	18.55 ± 5.40	0.73 ± 0.11	8.82 ± 1.06	1.38 ± 0.46	15.97 ± 7.79
Large Int.	0.76 ± 0.11	21.15 ± 8.55	0.58 ± 0.12	11.27 ± 1.82	1.79 ± 0.18	12.41 ± 7.50
Fat	1.21 ± 0.68	14.46 ± 5.71	2.06 ± 1.06	3.55 ± 1.37	2.19 ± 1.19	9.92 ± 4.09
Muscle	0.58 ± 0.24	28.26 ± 5.49	0.53 ± 0.03	12.00 ± 1.49	0.62 ± 0.26	33.13 ± 5.06
Bone	2.50 ± 1.08	7.08 ± 3.93	1.75 ± 0.36	3.74 ± 0.81	2.18 ± 1.58	10.88 ± 4.46
Skin	1.40 ± 0.57	11.49 ± 1.79	1.77 ± 0.57	3.80 ± 0.94	1.52 ± 0.13	13.75 ± 6.88

References

1. Patra M, Klingler S, Eichenberger LS, Holland J. Simultaneous Photoradiochemical Labelling of Antibodies for Immuno-PET. *iScience*. 2019;13:416-431.
2. Zanzonico P. Routine Quality Control of Clinical Nuclear Medicine Instrumentation: A Brief Review. *J Nucl Med*. 2008;49:1114-1131.
3. Fay R, Gut M, Holland JP. Photoradiosynthesis of 68Ga-Labeled HBED-CC-Azepin-MetMAb for Immuno-PET of c-MET Receptors. *Bioconjug Chem*. 2019;30:1814-1820.
4. Vosjan MJWD, Perk LR, Visser GWM, et al. Conjugation and radiolabeling of monoclonal antibodies with zirconium-89 for PET imaging using the bifunctional chelate p-isothiocyanatobenzyl-desferrioxamine. *Nat Protoc*. 2010;5:739-743.
5. Perk LR, Vosjan MJWD, Visser GWM, et al. P-Isothiocyanatobenzyl-desferrioxamine: A new bifunctional chelate for facile radiolabeling of monoclonal antibodies with zirconium-89 for immuno-PET imaging. *Eur J Nucl Med Mol Imaging*. 2010;37:250-259.
6. Holland JP, Divilov V, Bander NH, Smith-Jones PM, Larson S, Lewis JS. ^{89} Zr-DFO-J591 for immunoPET of prostate-specific membrane antigen expression in vivo. *J Nucl Med*. 2010;51.
7. Lindmo T, Boven E, Cuttitta F, Fedorko J, Bunn PA. Determination of the immunoreactive function of radiolabeled monoclonal antibodies by linear extrapolation to binding at infinite antigen excess. *J Immunol Methods*. 1984;72:77-89.
8. Institute for Laboratory Animal Research. Guide for the Care and Use of Laboratory Animals: 8th Ed.; 2011.
9. Fridman R, Benton G, Aranoutova I, Kleinman HK, Bonfil RD. Increased initiation and growth of tumor cell lines, cancer stem cells and biopsy material in mice using basement membrane matrix protein (Cultrex or Matrigel) co-injection. *Nat Protoc*. 2012;7:1138-1144.
10. Bai B, Dahlbom M, Park R, et al. Performance comparison of GENISYS4 and microPET preclinical PET scanners. *IEEE Nucl Sci Symp Conf Rec*. 2012;bai:3765-3768.